J. metamorphic Geol., 1996, **14,** 591–611

Genesis of the Kapuskasing (Ontario) migmatitic mafic granulites by dehydration melting of amphibolite: the importance of quartz to reaction progress

T. H. D. HARTEL* AND D. R. M. PATTISON
Department of Geology and Geophysics, University of Calgary, Calgary, Alberta, Canada T2N 1N4

ABSTRACT Migmatitic, granulite-grade mafic gneisses make up a significant part of the Kapuskasing Structural Zone (KSZ), Ontario. Although they contain a common mineral assemblage [hornblende (Hbl) + plagioclase (Pl) + diopside (Di) ± garnet (Grt) + quartz (Qtz) ± titanite (Ttn)], the mafic gneisses show wide variations in modal mineralogy from hornblende-rich to diopside + garnet-rich varieties and all gradations between. Up to 25 vol.% segregated plagioclase + quartz-rich (trondhjemitic) leucosome (Tdh) is intimately associated with the mafic gneiss, occurring in a continuum of patches, veins and transecting dykes at scales ranging from decimetres to micrometres. The texture and composition of the leucosome, combined with *P-T* estimates for the host rocks above the solidus, suggest it represents crystallized trondhjemitic melt. Quartz is mainly restricted to the segregated leucosomes but more rarely occurs in a variety of interstitial textures in the mafic gneiss, suggesting that it crystallized from a melt phase rather than having been present as a solid phase at peak metamorphic conditions. Modal and textural data indicate a reaction relationship of the form: Hbl + Pl(+ Qtz?) = Grt + Di + Ttn + leucosome (Tdh), implying that the granulite-forming process involved dehydration melting of an amphibolite protolith. Pressure-temperature estimates from Grt + Di + Pl + Qtz geothermobarometry are 9 kbar and 685-735 °C; however, based on experimental studies of dehydration melting of amphibolite, we estimate that peak conditions were closer to 11 kbar, 850 °C. Mass balance analysis, using the technique of singular value decomposition, and reaction space analysis were used to quantify the reaction and to determine the controls on reaction progress. The following mass balance provides a model for the natural reaction:

$$1.00\ \mathrm{Hbl} + 0.92\ \mathrm{Pl} + 3.76\ \mathrm{Qtz} = 1.14\ \mathrm{Grt} + 1.54\ \mathrm{Di} + 0.21\ \mathrm{Ttn} + 1.49\ \mathrm{Tdh} + 0.14\ \text{`pg'} + 0.39\ \mathrm{Fe_{-1}Mg} + 0.33\ \mathrm{NaSiCa_{-1}Al_{-1}}$$

where 'pg' is a pargasite-like exchange. In all model mass balances tested, quartz is a reactant with a large coefficient. We argue that the abundance of quartz in the amphibolite protolith was the primary control on the differing extents of reaction observed. Mineral compositional variation exerted a secondary control on reaction progress, with Fe-richer layers containing An-richer plagioclase and more actinolitic amphibole reacting earliest (i.e. at lowest temperatures). Comparison of the calculated amount of melt produced in the gneisses with that now observed implies expulsion of 5–30% of the melt. These volumes are similar to those predicted from REE modelling of Archaean tonalities and trondhjemites from a garnet amphibolite source, suggesting that the KSZ mafic gneisses may be representative of partially depleted source rocks for trondhjemite-tonalite generation.

Key words: amphibolite; dehydration melting; granulite; mass balance analysis; migmatite; quartz, reaction progress.

INTRODUCTION

The process of dehydration melting (Thompson, 1982) involves the incongruent reaction of hydrous minerals (e.g. micas and amphiboles) to form simultaneously anhydrous minerals (e.g. garnet and pyroxenes) and a quartzofeldspathic melt phase (e.g. Powell, 1983; Waters, 1988; Pattison, 1991). Dehydration melting reactions can be represented by the addition of a vapour-producing dehydration reaction (1) and a vapour-consuming melting reaction (2) such that free water as a phase is eliminated, e.g.

$$\mathrm{Pl} + \mathrm{Hbl} + \mathrm{Qtz} = \mathrm{Di} + \mathrm{Grt} + \mathrm{H_2O} \quad (1)$$

$$\mathrm{Pl} + \mathrm{Qtz} + \mathrm{H_2O} = \text{trondhjemitic melt} \quad (2)$$

$$\mathrm{Hbl} + \mathrm{Pl} + \mathrm{Qtz} = \mathrm{Di} + \mathrm{Grt} + \text{trondhjemitic melt} \quad (3)$$

(abbreviations from Kretz, 1983). A significant feature of dehydration melting reactions is that a_{H_2O} is buffered

Correspondence: pattison@geo.ucalgary.ca
*Present address: Brandley Consulting, 4528 41st St. SW, T3A 0N2, Calgary, Alberta, Canada.

to fixed values (or, in the case of multivariancy, to restricted values) when the complete reaction assemblage is present (Clemens & Vielzeuf, 1987). This contrasts with vapour-releasing subsolidus dehydration reactions or vapour-consuming melting reactions whose location in P–T space can be displaced by varying a_{H_2O}. In the absence of fluid infiltration, simple heating will inevitably lead to dehydration melting regardless of the initial a_{H_2O} (see T–a_{H_2O} diagram in Pattison, 1991).

Dehydration melting provides an appealing mechanism to form simultaneously granulite facies rocks (anhydrous residues of the melting process) and granitoid melts (Brown & Fyfe, 1970), the latter which may segregate and migrate upwards in the crust. From a field perspective, first-order evidence in support of dehydration melting as a common granulite-forming mechanism is the common occurrence in granulites of segregated quartzofeldspathic leucosomes, at scales ranging from submillimetre to 1-10s of metres (migmatitic granulites). Many of the structural and textural features of leucosomes in migmatitic granulites suggest that they were at one time wholly or partially fluid. Combined with their quartzofeldspathic (granitoid) composition and P–T estimates of their host rocks above the wet solidus, the evidence strongly suggests that the leucosomes represent crystallized silicate melt.

There has been comparatively little work done on granulite-grade migmatization processes in mafic (metabasic) systems compared with the large number of theoretical, experimental and field-based studies on metapelitic systems (e.g. Ashworth, 1976; Brown, 1979; Thompson, 1982; Vielzeuf & Clemens, 1987; Waters, 1988; Patino-Douce & Johnson, 1991; Pattison, 1991; Nyman *et al*., 1995; and references therein). Constraints on phase relations, melt compositions and melt volumes for K-poor metabasic rocks undergoing vapour-absent dehydration melting are provided by the experimental studies of Ellis & Thompson (1986), Beard & Lofgren (1991), Rushmer (1991), Rapp *et al.* (1991), Wolf & Wyllie (1991, 1993), Thompson & Ellis (1994) and Patiño-Douce & Beard (1995). Field-based studies of migmatitic mafic granulites include those of Percival (1983), Tait & Harley (1988), Beard (1990), Sawyer (1991) and Williams *et al.* (1995).

The purpose of this study is to determine controls on the genesis of migmatitic mafic granulites using as a natural example the mafic gneisses of the Kapuskasing Structural Zone (KSZ), Ontario (Percival, 1983; see also *Canadian Journal of Earth Sciences*, 1994, Vol. 31, no. 7). Although showing a common mineral assemblage (Hbl + Pl + Qtz ± Grt + Di ± Ilm ± Ttn), the gneisses show a particularly wide range of modal mineralogy within small outcrop-sized areas, ranging from hornblende + plagioclase-rich layers to Grt + Di + plagioclase-rich layers and all gradations between (Percival, 1983). A variety of plagioclase + quartz-rich (trondhjemitic) leucosomes of various types and scales occur within the gneisses. The modal variability of the mafic gneisses makes them ideal for investigating granulite-forming processes over a range of mafic compositions in which pressure and temperature can safely be assumed to have been the same.

Specific goals of the study are (1) to search for textural and modal mineralogical evidence either in support of or against granulite and migmatite formation by dehydration melting; (2) to determine the integrated whole-rock reaction or reactions accounting for the observed mineral assemblages and textures; and (3) to account for the variable modal mineralogy between adjacent layers. We use combined modal and textural observations to infer qualitatively, and mineral chemistry and mass balance analysis to model quantitatively the granulite + leucosome-producing reaction(s). The observed features are shown to be well modelled by differing extents of reaction of essentially one common dehydration-melting reaction. We argue that the primary control on extent of reaction was abundance of quartz in the protolith, with mineral compositional variation between layers exerting a secondary control.

GEOLOGICAL SETTING

The Kapuskasing Structural Zone (Percival, 1983; Percival & West, 1994) cuts obliquely across the EW-trending subprovinces of the Archaean Superior craton. The KSZ comprises high-grade metamorphic rocks and is marked by strong positive gravity and aeromagnetic anomalies. The KSZ has an elongate surface expression at least 50 km wide and 500 km long. It trends NNE from the north-eastern shore of lake Superior towards the southern tip of James Bay, where the structure disappears under a cover of Phanerozoic sediment (Fig. 1).

The KSZ is interpreted as an uplifted portion of the Archaean continental crust (Percival, 1983). It was thrust eastward and upward over greenschist facies rocks of the Abitibi subprovince along a series of W-dipping crustal-scale thrust faults (Geis *et al*., 1990) whose surface expression is represented by the Ivanhoe Lake shear zone (Bursnall *et al*., 1994). The overall structure is interpreted to represent an intracratonic uplift related to Hudsonian collision (Percival & West, 1994). Although having experienced a range of magmatic and metamorphic events between 2700 and 2585 Ma, the main stage of high-grade metamorphism occurred about 2660 Ma (Corfu, 1987; Krogh & Moser, 1994). The age of major uplift along the Ivanhoe Lake fault remains uncertain, with ages between 2450 and 1930 Ma having been suggested (Hanes *et al*., 1994; Krogh & Moser, 1994; Percival & Peterman, 1994).

Setting and location of outcrops

The southern part of the KSZ, between Chapleau and Foleyet, consists of NE-striking, NW-dipping belts of paragneiss, migmatitic mafic gneiss, ultramafic gneiss, dioritic to tonalitic gneiss and locally gneissic meta-anorthosite (Thurston *et al*., 1977; Percival, 1983). Mafic rocks are characterized by Grt + Di ± Opx mineral assemblages, indicative of high-pressure granulite-grade metamorphism (Percival, 1983). To the NW, lower grade mafic rocks are diopside-bearing but garnet-absent (fig. 3 of Percival, 1983).

Clean exposures of migmatitic mafic gneiss are found in outcrops along Highway 101 between Foleyet and Chapleau (Percival, 1986) and in water-blasted outcrops near Harold Lake just off the Warren-Carty logging road, about 2.5 km north of Highway 101 (Fig. 1). The Warren-Carty exposures are the primary focus of this study. Despite their location *c.* 2 km from the metamorphosed Shawmere

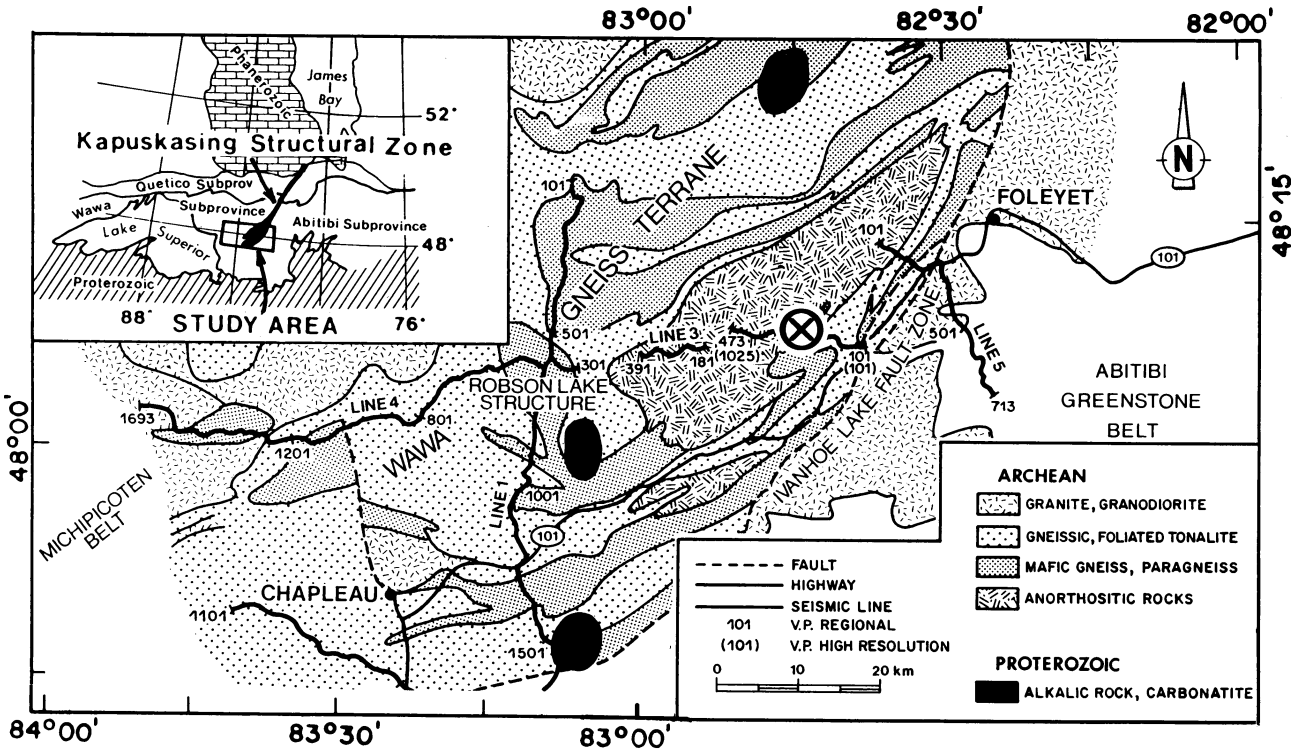

Fig. 1. Geological map of the high-grade rocks of the Kapuskasing Structural Zone (from Geis *et al.*, 1990; based on Percival & Card, 1983), showing the location of the outcrops discussed in this study (cross inside circle). The solid numbered lines are the location of seismic lines discussed in Geis *et al.* (1990).

Anorthosite (Fig. 1), the mafic gneisses show the same range of mineralogy and textures as mafic gneisses elsewhere in the KSZ, and are therefore thought to owe their metamorphic characteristics to regional processes.

OUTCROP FEATURES OF MIGMATITIC MAFIC GNEISSES

Outcrops of migmatitic mafic gneiss show strong layering on a centimetre to decimetre scale (Fig. 2A–C). Interlayered with the mafic gneisses are Pl + Qtz + Hbl ± Bt ± Di ± Grt tonalitic gneisses, in addition to rarer ultramafic Hbl ± Di ± Opx ± Grt gneisses and Pl + Bt + Qtz ± Grt ± Opx paragneisses. Within the mafic gneisses, there are two principal domains (Fig. 2): melanosome and leucosome (terms from Ashworth, 1985).

Melanosome

The melanosome makes up the bulk (>80%) of the mafic gneiss and primarily defines the layering in the outcrops. The layers range from hornblende-plagioclase-rich varieties to plagioclase-diopside-garnet-rich varieties, with all gradations between (Fig. 2A). Despite the large modal variations, the mineral assemblage in the melanosome layers is relatively uniform: Hbl + Pl ± Grt + Di + Qtz, with variable amounts of titanite and rare ilmenite, biotite and epidote. Most rock types have a weak to strong foliation that dips shallowly to the WNW (Percival, 1983). Based on field characteristics and whole-rock chemistry, the layering in the mafic gneisses is interpreted to be primary, most likely representing metamorphosed basaltic lava flows and/or sills (Percival, 1986).

Leucosome

White plagioclase + quartz-rich leucosomes within the darker melanosome layers give the rock its migmatitic appearance (Fig. 2). Leucosome is more abundant in the hornblende-richer layers than in the garnet + diopside-richer layers (Fig. 2A). Many of the leucosomes, especially in the hornblende-rich layers, show little evidence for solid-state deformation. Grain size in the leucosome is generally coarser than in the enclosing mafic gneiss, and increases as the size of the leucosome increases. The proportion of Pl/Qtz in the leucosomes ranges from 50-65:50-35, characteristic of trondhjemite. The same range of mafic minerals occurs in the leucosomes as in the melanosome, including diopside, garnet and hornblende, and rarely biotite and epidote (Fig. 2D).

The leucosome occurs in a variety of forms with respect to degree of continuity (length) and degree of parallelism to compositional layering (Fig. 2). Examples of continuous concordant leucosomes are seen in Fig. 2(A,B), whereas continuous discordant

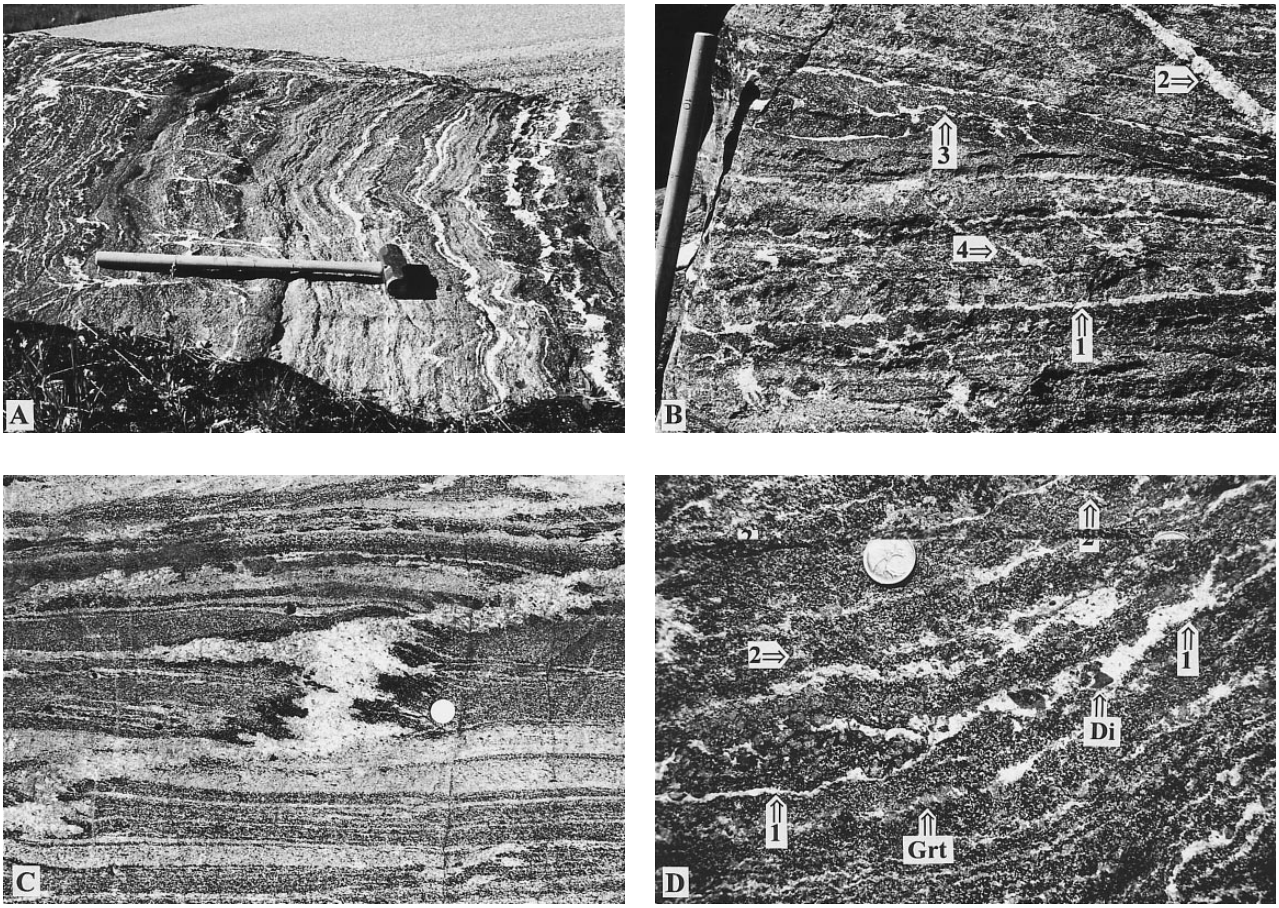

Fig. 2. Outcrop photographs of migmatitic mafic gneisses. (A) Interlayered mafic gneiss (dark-medium grey) with abundant quartzofeldspathic leucosome (white). The darkest layers are hornblende-rich, whereas the lighter grey layers are richer in garnet and diopside. Note the variations in distribution, size and continuity of leucosomes. Divisions on the hammer are 10 cm. (B) Layered mafic gneiss showing details of different types of leucosomes: continuous, layer-parallel leucosome (1); continuous, cross-cutting leucosome (2); small, discontinuous, layer-parallel leucosome contained within individual layers (3); small, discontinuous, incipiently cross-cutting leucosome (4). Leucosome types commonly, but not always, show continuous transitions with each other. Note the greater abundance of leucosome in the hornblende-richer (darker) layers. Divisions on the hammer are 10 cm. (C) Trondhjemitic vein (white) cross-cutting interlayered mafic (dark) and tonalitic (light grey) gneiss. Note the dark hornblende-rich margins against the vein where it cross-cuts the Grt + Di-bearing mafic gneiss. This feature is suggestive of late, retrograde hydration of the mafic gneiss, interpreted to be due to hydrous fluid release from the trondhjemitic vein when it crystallized. Coin is 2.6 cm in diameter. (D) Detail of leucosome development in mafic gneiss. Notice the range of scales of development of leucosome, from obvious discrete segregations several cm in length (1) to almost imperceptible segregations, mm in size, which merge into the mafic host rock (2). Notice also the occurrence of garnet and diopside within both the mafic host rock and the leucosome. Coin is 2.3 cm in diameter.

leucosomes are illustrated in Fig. 2(B,C). The discordant leucosomes have the appearance of dykes and veins that have been injected into the mafic gneisses (e.g. Fig. 2C). Some discordant leucosomes show continuous transitions with concordant and patchy leucosomes hosted in mafic gneiss, suggesting that a portion of the discordant leucosome is locally derived. A number of discordant leucosomes show dark, coarse-grained hornblende-rich margins against the enclosing mafic gneiss (Fig. 2C).

Discontinuous leucosomes show a variety of aspect ratios from elongate to rounded and patchy (Fig. 2B,D). In some rocks, leucosome has accumulated in dilatant zones such as in boudin necks and in what appear to be shear bands, whereas in others the leucosome occurs as pods and lenses within the relatively homogeneous groundmass. In places the leucosomes appear to be completely isolated (in two dimensions), but more typically they show evidence for incipient connectivity with other relatively isolated leucosomes and with more continuous leucosomes (Fig. 2B,D). The size of the leucosomes ranges from several centimetres in width and tens of centimetres in length down to millimetre-scale segregations with only a few grains of plagioclase and quartz. These latter leucosomes merge imperceptibly into the Hbl + Pl + Grt + Di-rich mafic host gneiss (Fig. 2D). This continuity of scales suggests an internal origin for

the leucosome, a view supported by the relative uniformity in the texture and mineralogy in the different leucosome types.

The overall impression of the distribution, connectivity and continuity of scales of the leucosome is that of an internally derived fluid material that was variably segregated into pods, dilatant zones and fractures. The plagioclase + quartz-rich nature of leucosome, combined with *P–T* estimates above the wet solidus of plagioclase + quartz (see below), suggests that the fluid was a silicate melt phase of trondhjemitic composition. The intimate occurrence of the leucosome within the gneisses and the apparent stability of garnet and diopside in many leucosomes (e.g. Fig. 2D) suggests that at some point the leucosome material was stable with the solid granulite assemblage. On the other hand, the hornblende-rich margins typically developed against discontinuous leucosomes (e.g. Fig. 2C) is suggestive of local rehydration of the garnet + diopside-bearing host gneiss, most likely from water that was released from the trondhjemitic melt during crystallization.

PETROGRAPHY

Modal mineralogy

Seven samples of mafic gneiss were selected for point counting, covering the range of melanosome compositions from hornblende-rich to garnet + diopside-rich. The aim was to restrict the point counting to portions of the gneiss away from obvious segregated leucosome, although in some samples it was difficult to discern melanosome-leucosome contacts. The results are plotted in Fig. 3. A negative correlation between hornblende and each of plagioclase, diopside, garnet and titanite is seen. quartz shows no consistent modal pattern with respect to hornblende (see discussion below).

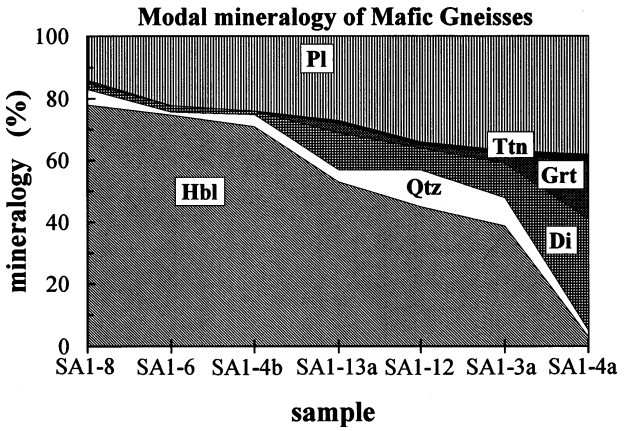

Fig. 3. Area chart showing modal mineralogy of the seven melanosome layers discussed in the paper.

Textures of garnet, diopside and titanite

Within the hornblende-rich layers, the texture is generally granoblastic apart from a weak lineation defined by preferential orientation of hornblende. The garnet + diopside-rich layers show a generally granoblastic texture. Grain size in all layer types ranges from 0.2 to 3 mm, averaging 1-2 mm.

Figure 4 shows textures of garnet, diopside and titanite. Garnet porphyroblasts in the gneisses range from inclusion-poor to inclusion-rich. Figure 4(A) shows garnet porphyroblasts with anhedral-euhedral grain boundaries that contain inclusions of optically continuous hornblende and rarer plagioclase. In contrast to the generally granoblastic texture of garnet, Fig. 4(B) shows skeletal garnet between hornblende grains that merges into a larger, inclusion-bearing garnet porphyroblast. Diopside shows a similar range of textures to garnet (Fig. 4C,D). Diopside is generally granoblastic, locally with inclusions of plagioclase and hornblende (Fig. 4c). Rarer skeletal diopside is found along contacts between hornblende grains (Fig. 4d) or between hornblende and plagioclase grains. Titanite is generally inclusion free, but locally contains hornblende inclusions (Fig. 4E), and also occurs as small grains along hornblende-hornblende contacts (Fig. 4B,F) or rarely on the margins of ilmenite crystals (Fig. 4B).

In some samples, garnet and diopside porphyroblasts show all gradations between skeletal, poikiloblastic and inclusion-free textures. The range of textures is interpreted to represent different stages in the progressive growth of garnet, diopside and titanite at the expense of hornblende and plagioclase. Initial growth of garnet and diopside occurred along margins of hornblende (skeletal textures; Fig. 4B,D,F); with increased reaction progress, porphyroblasts developed (Fig. 4A,C,E).

Distribution and texture of quartz and plagioclase-quartz segregations

The bulk of the quartz in the mafic gneisses occurs in macroscopic plagioclase + quartz segregations (leucosomes) of varying scales. However, small amounts of quartz occur locally in the melanosome. The distribution and textures of quartz contrasts with those for hornblende, garnet, diopside and titanite. Microscopic plagioclase + quartz-rich segregations (microleucosomes) and plagioclase + quartz-rich film-like intergrowths show a number of similarities to the distribution and textures of quartz, so they are described together.

Description

Figure 5 shows textures of quartz, plagioclase + quartz microleucosomes and plagioclase + quartz films. Figure 5(A) shows the margin between a

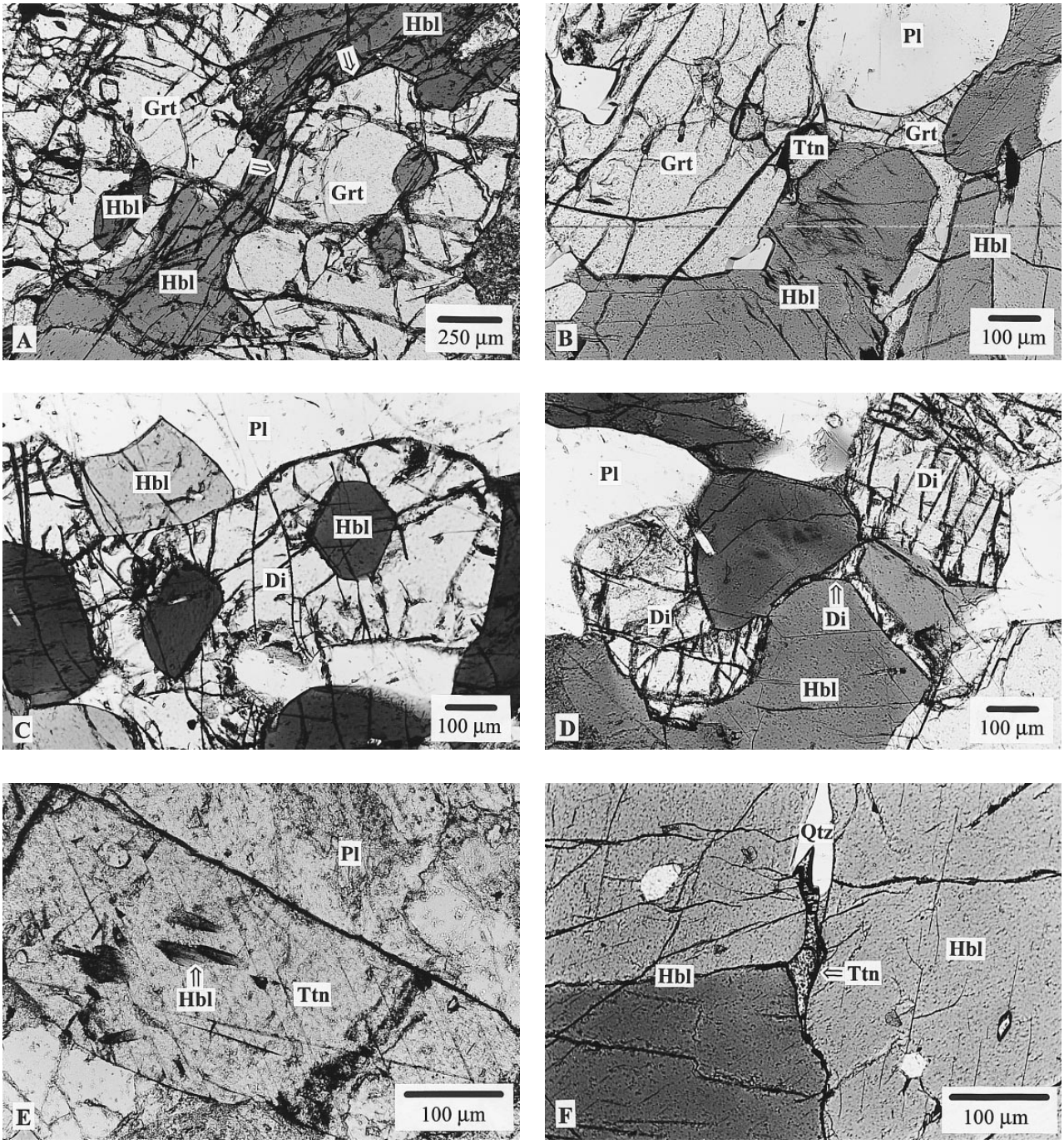

Fig. 4. Photomicrographs of garnet, diopside and titanite. (A) Garnet porphyroblasts with inclusions of hornblende, the latter which are optically continuous with the remnant hornblende running diagonally. Notice the euhedral margin of the garnet porphyroblast against the hornblende (arrow), suggesting that the garnet grew at the expense of hornblende. (B) Skeletal garnet between hornblende crystals that is continuous with larger garnet porphyroblast. Small crystals of titanite are also developed at the hornblende margins. (C) Diopside porphyroblast showing inclusions of hornblende, some of which are optically continuous. (D) Skeletal diopside between hornblende crystals that grades into coarser-grained diopside crystals. (E) Titanite crystal containing inclusions of hornblende. (F) Small titanite crystal developed at a triple junction between hornblende crystals and adjacent to a thin quartz 'film' between hornblende crystals.

plagioclase + quartz-rich leucosome and hornblende-rich host gneiss. Of special note are a number of irregularly shaped, generally elongate intergrowths of mainly quartz with lesser plagioclase that extend from the main leucosome between hornblende crystals in the melanosome. Figure 5(B) shows a coarse-grained, irregularly shaped quartz crystal on the margin of a leucosome adjacent to a medium-grained, granoblastic

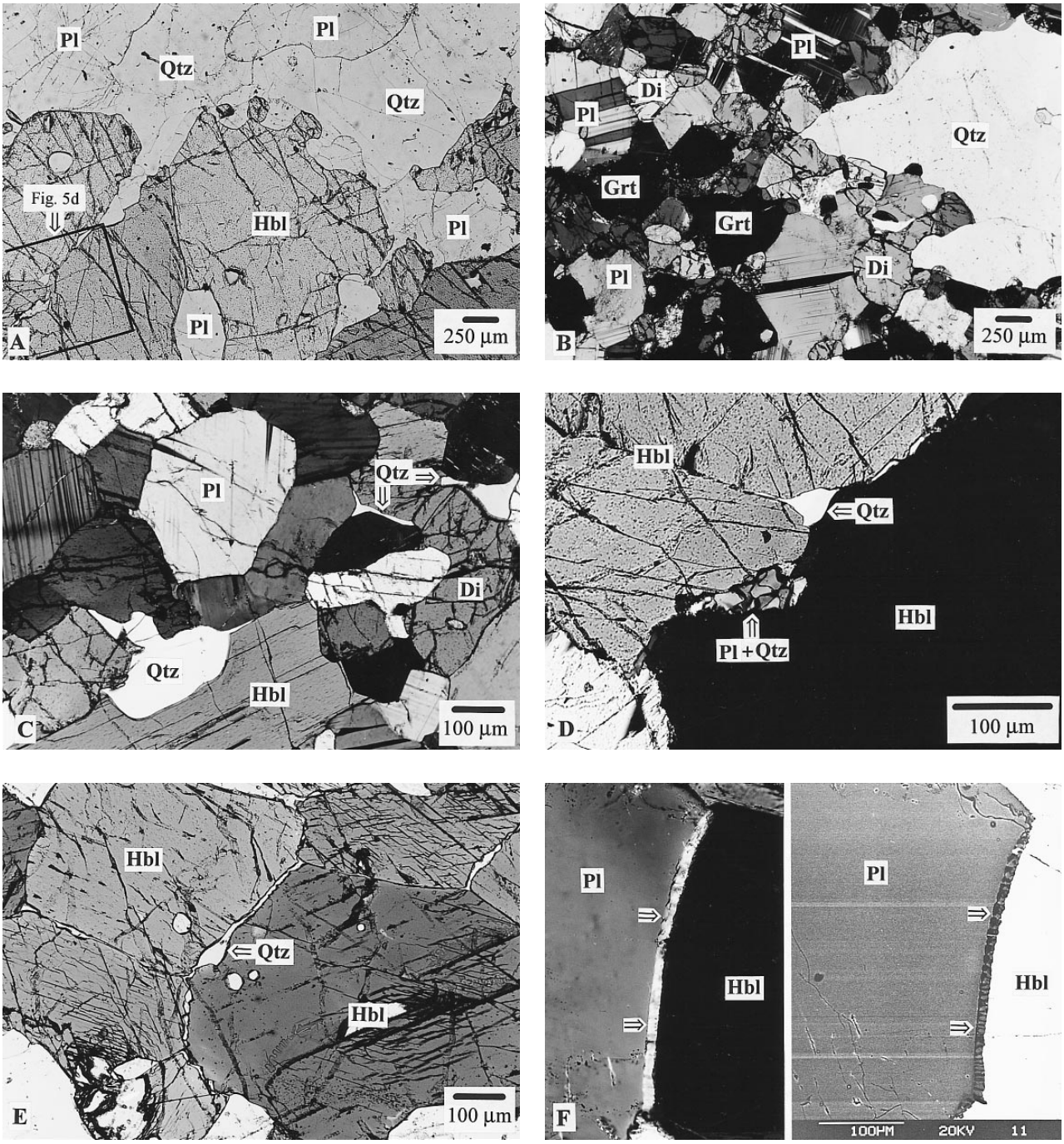

Fig. 5. Photomicrographs of quartz and quartz-plagioclase films. (A) Margin between Qtz-Pl leucocratic segregation (upper part) and hornblende-rich melanosome (lower part). Notice the smooth transition from coarse-grained intergrown Pl + Qtz with curvilinear margins in the leucocratic segregation to narrower necks and intergranular pockets of Pl + Qtz between hornblende crystals. (B) Margin between leucocratic Pl + Qtz segregation (right side) with Cpx + Pl + Hbd + Grt melanosome (left side). Note the contrast between the large, irregularly shaped, optically continuous quartz grain in the leucosome compared with the finer-grained, generally granoblastic texture of plagioclase, diopside, garnet and hornblende in the melanosome. (C) Textures in melanosome. The overall texture of the melanosome is granoblastic, with the exception of quartz which occurs interstitially in small, irregularly shaped crystals with high surface to volume ratio between the other minerals. (D) Enlargement of (A). Interstitial quartz is developed at a triple junction between three hornblende crystals and along hornblende grain margins. Below the quartz is a pocket of fine-grained, intergrown plagioclase + quartz between two hornblende crystals. (E) Quartz 'films' with high surface to volume ratios occurring between hornblende crystals. Such films typically show smooth transitions into coarser Pl + Qtz segregations. (F) Photomicrograph (left side) and back-scattered electron image (right side) of a Pl + Qtz 'film' between one hornblende and several plagioclase crystals. The film consists of finely intergrown 'droplets' of plagioclase and quartz (see Fig. 8 for a compositional profile through a similar film).

intergrowth of plagioclase, garnet and diopside (melanosome).

Figure 5(C,D) show two examples of interstitial textures of quartz. In Fig. 5(C), the quartz occurs principally along grain margins of hornblende, plagioclase and diopside and, in one place, occupies a triple junction between hornblende, diopside and plagioclase. Figure 5(D), an enlargement of a portion of Fig. 5(A), shows interstitial quartz at a triple junction of three hornblende crystals in addition to a plagioclase + quartz microleucosome between two hornblende crystals. Figure 5(E) shows several elongate quartz films between hornblende and plagioclase grains. All of the above types of quartz show irregular, nongranoblastic textures with high surface-volume ratios.

Figure 5(F) shows an optical image and a backscattered electron image of a plagioclase + quartz film between a plagioclase and hornblende grain. Several rocks contain these films. The films typically show continuous transitions into plagioclase + quartz microleucosomes and interstitial quartz grains. The films consist primarily of vermicular or droplet shaped quartz with plagioclase between. Quartz and plagioclase become more equidimensional with increasing film width. The average width and length of 70 plagioclase-quartz films are 0.009 and 0.2 mm, respectively.

Interpretation

The interstitial, curvilinear quartz textures with high surface-volume ratios contrast with the predominantly granoblastic textures of the other minerals in the rock and suggest a different mode of origin. Textures such as these have been described in migmatites by Pattison & Harte (1988), Vernon & Collins (1988), Grant & Frost (1990) and Harte *et al.* (1991). These authors interpreted the quartz textures as magmatic, with the interstitial quartz mimicking melt pockets between solid grains (intercumulus texture). The interstitial quartz, plagioclase + quartz microleucosomes and plagioclase + quartz films are reminiscent of melt textures in the partial melting experiments of Mehnert *et al.* (1973), Paquet & Francois (1980), Jurewicz & Watson (1984), Hacker (1990) and Wolf & Wyllie (1991), in which glass from quenched runs showing small degrees of partial melting occurs principally at triple junctions and along grain boundaries of the reactant solid phases.

Consequently, it may be that most or possibly all of the quartz now observed in the rocks was not solid at the time of peak metamorphism, instead having precipitated from the trondhjemitic melt phase on cooling from peak metamorphic conditions. The small amounts of interstitial quartz in the melanosome may represent small volumes of fractionated melt that were not expelled from the groundmass (analogous to intercumulus orthopyroxene between cumulus olivine + chromite crystals in ultramafic complexes).

Relation to other textures

The quartz and plagioclase + quartz microtextures extend the continuity of scales of leucosome development noted at outcrop scale (decimetre-millimetre) to the microscopic scale (millimetre-micrometre), and provide further evidence for an internal origin for the leucosome. The skeletal nature of the quartz and plagioclase + quartz films, and their occurrence along grain margins of hornblende and plagioclase, resembles the skeletal garnet and diopside textures noted above, and suggests a related mode of origin. Small crystals of garnet, diopside and titanite sometimes occur in or along the margins of plagioclase + quartz microleucosomes and films, analogous to the occurrence of these minerals in leucosomes at outcrop scale (e.g. Fig. 2D).

Although the above features are relatively common, many rocks show no evidence for skeletal diopside and garnet or for thin plagioclase + quartz microleucosomes. The most likely explanation is that these delicate textures were destroyed by later deformation.

Interpretation of modal mineralogy and textures as products of dehydration melting

Summarizing the above observations, the modal mineralogy and outcrop/thin-section textures provide strong evidence for the reaction of hornblende and plagioclase to form garnet, diopside and titanite. The composition and texture of plagioclase + quartz-rich leucosomes and films suggest that they represent crystallized trondhjemitic melt. The continuity of scales of leucosome development from micrometre to decimetre scale is consistent with an internal origin for the melt within the mafic gneiss. The apparently stable occurrence of garnet, diopside and titanite in or adjacent to the leucosome is suggestive of the leucosome having been stable with the anhydrous granulite product assemblage at some point.

These features can be reconciled in a process involving dehydration melting of a hornblende-rich protolith, such as by the following generalized reaction:

$$\mathrm{Hbl} + \mathrm{Pl}(+\mathrm{Qtz?}) = \mathrm{Grt} + \mathrm{Di} + \mathrm{Ttn} + \mathrm{Pl} + \mathrm{Qtz\text{-}leucosome\ (Tdh)}. \quad (4)$$

Reaction (4) is very similar to the reaction proposed by Percival (1983). Based on modal mineralogy alone, the role of quartz is uncertain. We examine the role of quartz below.

MINERAL CHEMISTRY

Mineral chemical analyses of garnet, diopside, hornblende, plagioclase and titanite from each of the seven samples in Fig. 2 are listed in Tables 1–5, respectively. Graphs of variations in selected compositional parameters as a function of modal mineralogy are provided in Fig. 6. Microprobe operating conditions were the same as listed in Pattison (1991). Typical detection limits and analytical precisions are given in Nicholls & Stout (1988) and Pattison (1991).

Table 1. Summary of electron microprobe analyses of garnet.

	SA1-3a	SA1-4a	SA1-8	SA1-12	SA1-13
SiO_2	37.50	37.87	37.93	37.86	37.68
TiO_2	0.03	0.05	0.03	0.03	0.03
Al_2O_3	20.21	20.44	20.93	20.66	20.77
FeO	26.30	27.44	26.36	26.47	26.85
MnO	2.94	1.41	2.50	2.44	2.33
MgO	3.25	3.18	3.87	3.58	3.56
CaO	9.45	10.38	9.21	9.41	9.15
Total	99.65	100.77	100.82	100.44	100.36
Si	2.995	2.991	2.981	2.991	2.981
Al	1.903	1.903	1.939	1.923	1.937
Ti	0.002	0.003	0.002	0.002	0.002
Fe	1.757	1.812	1.732	1.749	1.777
Mn	0.199	0.095	0.166	0.163	0.156
Mg	0.387	0.374	0.453	0.421	0.420
Ca	0.809	0.878	0.776	0.797	0.775
X_{Alm}	0.56	0.57	0.55	0.56	0.57
X_{Sps}	0.06	0.03	0.05	0.05	0.05
X_{Prp}	0.12	0.12	0.14	0.13	0.13
X_{Grs}	0.26	0.28	0.25	0.25	0.25
X_{Mg}	0.18	0.17	0.21	0.19	0.19

Cations calculated for 12 oxygens.

Table 2. Summary of electron microprobe analyses of diopside.

	SA1-3a	SA1-4a	SA1-6	SA1-8	SA1-12	SA-13a
SiO_2	50.95	51.11	52.26	51.82	51.95	51.84
TiO_2	0.23	0.34	0.12	0.18	0.22	0.23
Al_2O_3	2.42	3.00	2.01	2.31	2.33	2.55
FeO	12.35	12.92	9.87	11.59	11.59	11.64
MnO	0.33	0.16	0.32	0.32	0.27	0.26
MgO	10.93	10.63	12.73	11.68	11.68	11.59
CaO	21.39	21.73	21.89	21.82	22.25	22.11
Na_2O	0.62	0.63	0.57	0.58	0.55	0.70
Total	99.21	100.52	99.76	100.28	100.84	100.92
Si	1.948	1.932	1.963	1.952	1.948	1.942
Al	0.109	0.134	0.089	0.102	0.103	0.113
Ti	0.007	0.010	0.003	0.005	0.006	0.007
Fe	0.395	0.408	0.310	0.365	0.363	0.365
Mn	0.011	0.005	0.010	0.010	0.009	0.008
Mg	0.623	0.599	0.713	0.655	0.653	0.647
Ca	0.876	0.880	0.881	0.880	0.894	0.888
Na	0.046	0.046	0.042	0.042	0.040	0.051
X_{Mg}	0.61	0.59	0.70	0.64	0.64	0.64

Cations calculated for 6 oxygens.

In the cation assignments for garnet, diopside and hornblende in Tables 1–3, Fe cations are calculated assuming all Fe is Fe^{2+}. Estimates of Fe^{3+} in garnet, diopside and hornblende were made assuming electroneutrality using the methods described in Pattison (1991, p. 323). Hornblende estimates are based on an average of the 13eCNK and 15eNK methods of Robinson *et al.* (1982). For garnet, diopside and hornblende, average calculated $Fe^{3+}/(Fe^{3+}+Fe^{2+})$ values are 0.08, 0.10 and 0.11, respectively (Hartel, 1993); these values may or may not be significant owing to the large uncertainties in the calculation schemes. Cosca *et al.* (1991) favour the 13eCNK method for Fe^{3+} estimation in amphibole, which for our hornblendes increases Fe^{3+} by about 0.2 cations and increases $Fe^{3+}/(Fe^{3+}+Fe^{2+})$ to about 0.2.

Mineral zoning and selection of analysis points

In slowly cooled high-grade rocks such as the KSZ mafic gneisses (Percival & Peterman, 1994), nonuniform re-equilibration of mineral compositions on cooling from peak conditions is expected (cf. Pattison & Bégin, 1994). To test this possibility, cores and rims

Table 3. Summary of electron microprobe analyses of hornblende.

	SA1-3a	SA1-4a	SA1-4b	SA1-6	SA1-8	SA1-12	SA1-13a
SiO_2	41.29	41.85	42.96	43.38	42.39	41.42	42.29
TiO_2	2.04	1.72	1.40	1.22	1.59	1.88	1.65
Al_2O_3	12.67	12.86	11.90	11.68	12.33	12.56	11.91
FeO	19.27	19.32	16.52	15.68	17.86	18.03	18.57
Cr_2O_3	na	0.11	0.06	na	0.07	0.07	0.06
MnO	0.22	0.10	0.23	0.22	0.21	0.19	0.18
MgO	8.33	8.06	10.01	10.75	9.06	8.64	9.15
CaO	11.81	11.84	11.68	11.86	11.57	11.67	11.81
Na_2O	1.56	1.44	1.41	1.49	1.55	1.45	1.55
K2O	1.09	1.17	0.87	0.74	0.82	1.07	0.81
F	1.10	bdl	0.09	0.09	0.09	0.08	bdl
Cl	na	0.02	bdl	na	0.01	bdl	bdl
Total	98.38	98.49	97.13	97.11	97.55	97.06	97.98
-O=Cl,F	0.04	0.00	0.04	0.04	0.04	0.03	0.00
Total	98.34	98.49	97.09	97.07	97.51	97.03	97.98
Si	6.257	6.322	6.473	6.507	6.404	6.318	6.392
Al	2.263	2.290	2.113	2.065	2.195	2.258	2.121
Ti	0.232	0.195	0.159	0.138	0.181	0.216	0.188
Cr	na	0.013	0.007	na	0.008	0.008	0.007
Fe	2.442	2.441	2.082	1.967	2.256	2.300	2.347
Mn	0.028	0.013	0.029	0.028	0.027	0.025	0.023
Mg	1.881	1.815	2.248	2.403	2.040	1.964	2.061
Ca	1.917	1.916	1.886	1.906	1.873	1.907	1.912
Na	0.458	0.422	0.412	0.433	0.454	0.429	0.454
K	0.211	0.225	0.167	0.142	0.158	0.208	0.156
F	0.048	bdl	0.043	0.043	0.043	0.039	bdl
Cl	na	0.005	bdl	na	0.003	bdl	bdl
X_{Mg}	0.44	0.43	0.52	0.55	0.47	0.46	0.47
X_{Fe3+}	0.11	0.07	0.11	0.13	0.10	0.08	0.14

Cations calculated for 23 oxygen equivalents. na = not analysed. bdl = below detection limit.

(outer 15 μm) were analysed from 4–6 different grains in each sample, with variations due to grain size and neighbouring mineral noted. Additional constraints on zoning patterns were provided by compositional (X-ray) maps on two samples.

To avoid obvious resetting problems at the rims, core compositions from the largest grains were selected for mass balance analysis and thermobarometry calculations. These are the values listed in Tables 1–5 and used in Fig. 6. However, as discussed below, we consider it unlikely that all elements in the cores of coexisting phases quenched in at the same time, let alone at peak metamorphic conditions.

Garnet

Within individual garnet grains, compositional zoning appears to be minor except within about 100–200 μm of the rims. X_{Ca} shows minor and irregular core-rim variation, with rims ranging from the same values as the cores to 0.02–0.03 higher. For Mg/(Mg+Fe), rims are consistently lower by 0.02–0.03. The noncoincidence of zoning in X_{Ca} and Mg/(Mg+Fe) is like that described by Pattison & Bégin (1994), which they ascribed to continued exchange of Fe-Mg after Ca in the garnet had been quenched in. Referring to Fig. 6(A), as the modal abundance of hornblende decreases, X_{Ca} increases from 0.26 to 0.29, whereas Mg/(Mg+Fe) decreases from 0.22 to 0.18. X_{Mn} shows no pattern with modal mineralogy, and averages about 0.05.

Diopside

Zoning in Mg/(Mg+Fe) is present within 50–100 μm of the rims, characterized by a core-rim increase of 0.02–0.03. Al zoning is irregular, most typically showing a decrease of about 0.03 Al cations towards the rims. Referring to Fig. 6(B), as the modal abundance of hornblende decreases, Mg/(Mg+Fe) shows an overall decrease from about 0.71 to 0.62, whereas Al cations show an increase from about 0.09 to 0.13 cations.

Table 4. Summary of electron microprobe analyses of plagioclase.

	SA1-3a	SA1-3b	SA1-4a core	SA1-4a rim	SA1-4b	SA1-4c	SA1-6	SA1-8	SA1-12	SA1-13a
SiO_2	58.09	58.74	56.77	59.95	58.46	58.75	58.04	57.75	57.10	56.66
TiO_2	bdl	bdl	bdl	bdl	na	bdl	bdl	bdl	bdl	na
Al_2O_3	26.41	26.13	27.63	26.24	26.79	26.24	26.43	26.80	27.34	27.29
FeO	0.04	0.05	0.08	0.25	0.07	bdl	0.06	0.05	0.08	0.08
MnO	na	na	bdl	bdl	bdl	bdl	na	bdl	bdl	bdl
MgO	0.00	bdl	bdl	bdl	bdl	bdl	0.00	bdl	bdl	bdl
CaO	8.10	7.94	9.70	7.98	8.46	8.06	8.32	8.80	9.23	9.38
Na_2O	7.01	7.16	6.01	6.90	6.78	7.18	6.89	6.52	6.28	6.23
K_2O	0.13	0.14	0.15	0.16	0.10	0.13	0.11	0.10	0.16	0.10
Total	99.78	100.15	100.34	101.49	100.66	100.40	99.86	100.02	100.20	99.74
Si	2.604	2.622	2.540	2.636	2.598	2.617	2.601	2.585	2.556	2.550
Al	1.395	1.374	1.458	1.362	1.403	1.378	1.396	1.414	1.443	1.447
Fe^{2+}	0.002	0.002	0.003	0.009	0.002	bdl	0.002	0.002	0.003	0.003
Ca	0.389	0.380	0.465	0.377	0.403	0.385	0.400	0.422	0.443	0.452
Na	0.609	0.619	0.521	0.588	0.584	0.620	0.599	0.566	0.545	0.544
K	0.007	0.008	0.009	0.009	0.005	0.008	0.006	0.006	0.009	0.006
X_{An}	0.39	0.38	0.47	0.39	0.41	0.38	0.40	0.42	0.44	0.45
X_{Ab}	0.61	0.62	0.52	0.60	0.59	0.61	0.60	0.57	0.55	0.54
X_{Or}	0.00	0.00	0.00	0.00	0.00	0.00	0.00	0.00	0.00	0.00

Cations calculated for 8 oxygens. na = not analysed. bdl — below detection limit.

Table 5. Summary of electron microprobe analyses of titanite.

	SA1-12	SA1-4a	SA1-3a
SiO_2	31.46	31.95	31.49
TiO_2	39.45	39.77	39.32
Al_2O_3	1.09	1.07	1.15
Cr_2O	0.05	0.05	bdl
FeO	0.74	0.57	0.66
MnO	0.06	0.05	0.08
MgO	bdl	bdl	bdl
CaO	26.87	26.83	25.90
Na_2O	bdl	bdl	bdl
K_2O	bdl	bdl	bdl
F	0.07	0.18	0.14
Total	99.78	100.47	98.74
−O = F	0.03	0.08	0.06
Total	99.75	100.39	98.68
Si	1.022	1.029	1.031
Ti	0.964	0.963	0.968
Al	0.042	0.041	0.044
Cr	0.001	0.001	bdl
Fe	0.020	0.015	0.018
Ca	0.936	0.926	0.908
Mn	0.002	0.001	0.002
F	0.007	0.018	0.015

Cations calculated for 5 oxygens.

Hornblende

Zoning in Mg/(Mg + Fe) is characterized by rims higher than cores by 0.01–0.04. Al zoning shows no consistent pattern, with some rims higher and others lower than the cores by 0.00–0.14 cations. Referring to Fig. 6(C), as the modal abundance of hornblende decreases, total Al cations show an increase from 2.05 to 2.25; Mg/(Mg + Fe) decreases from about 0.58 to 0.45; Ca cations show no significant variation; and Na + K shows a modest increase from 0.58 to 0.67.

Plagioclase and plagioclase-quartz films

Plagioclase from melanosome shows weak to strong normal zoning, with rims lower in An content by 0.03–0.10, averaging 0.04 (e.g. SA1-4a in Table 4). Apart from sample SA1-3a, An content increases from about An_{40} to about An_{47} as a function of decreasing hornblende content (Fig. 6D).

Figure 7 shows a step scan through the long dimension of a plagioclase-quartz film between a hornblende crystal and a plagioclase crystal (e.g. Fig. 5F). Several individual analyses in the profile most likely represent mixed analyses from adjoining fine-grained quartz and plagioclase crystals, with peaks in Si content representing quartz-dominated analyses. The Pl/Qtz ratio (*c.* 60:40) and the An content (32–40%, neglecting the higher An peak in some quartz-dominated analyses) indicate that the films are trondhjemitic in composition.

Plagioclase compositions in the different domains show distinct compositional ranges. The An content in hornblende-rich domains (39–47%) is intermediate between that of the trondhjemite leucosome and films (35–40%) and the garnet + diopside + plagioclase-rich domains (43–80%). In the garnet + diopside + plagioclase-rich domains the An contents are more variable than that in hornblende-rich domains. The relationship in which the An content of plagioclase in the segregated leucosome and films is lower than that in the melanosome is consistent with an anatectic origin for the leucosome (Johannes, 1983, and references therein).

The An content of plagioclase in small, discontinuous trondhjemitic leucosomes within the mafic gneiss is similar to that in continuous, cross-cutting trondhjemite bodies (30–38%). This supports the textural evidence suggesting that at least some of the cross-cutting veins and dykes owe their origin to leucosome generated in the mafic gneisses.

P–T–a_{H_2O} CONDITIONS

Pressure-temperature conditions from geothermobarometry were calculated from the subassemblage Grt–Di–Pl–Qtz using the data in Tables 1, 2 and 4, and are listed in Table 6. Complications in interpreting the results include the possibility of down-temperature resetting following the thermal peak, and uncertain a_{SiO_2} if quartz was not part of the solid assemblage at peak conditions.

Temperature

Temperature results based on Fe-Mg exchange between garnet and diopside using four different calibrations are listed in Table 6. The averages and ranges (in parentheses) are as follows (temperatures in °C): 745 (725–765) (Ellis & Green, 1979); 640 (615–660)

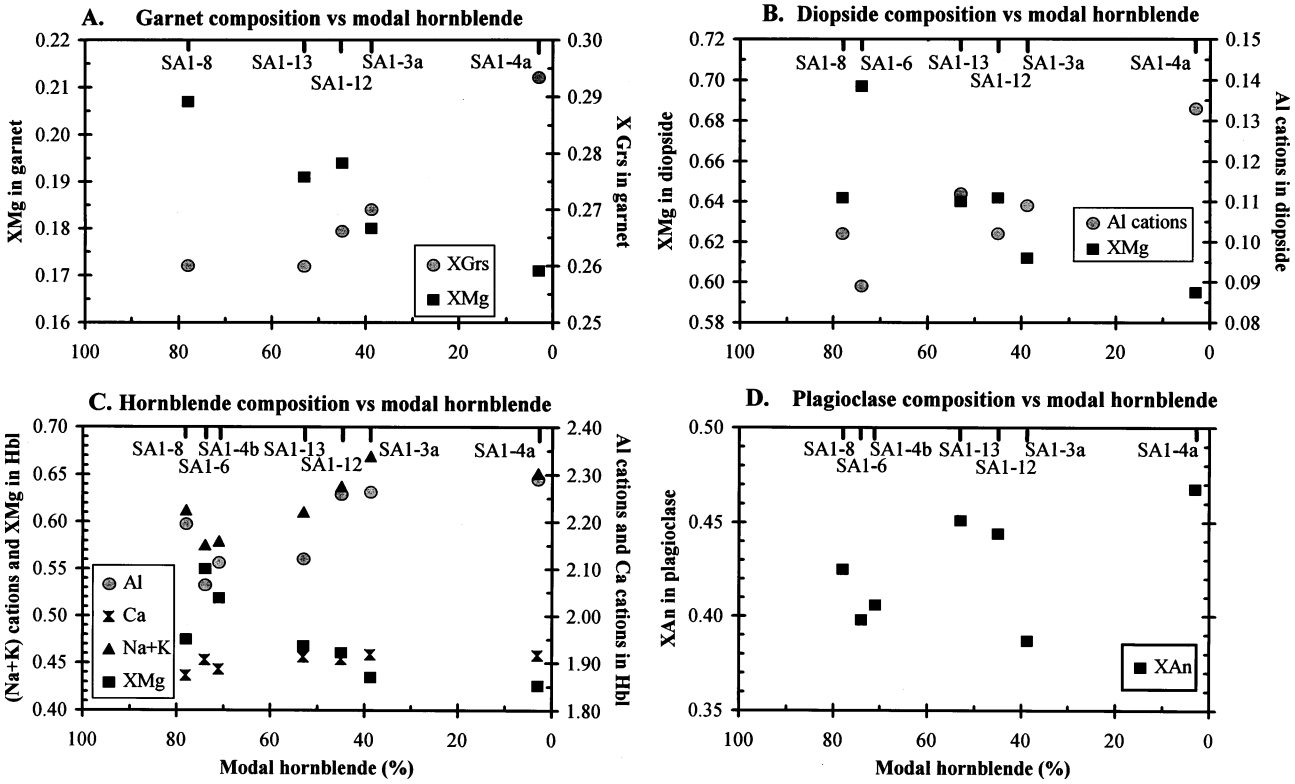

Fig. 6. Mineral compositional variations (core compositions) as a function of modal hornblende. Refer to Tables 1–4 for full chemical analyses. (A) Garnet. $X_{Mg} = Mg/(Mg+Fe)$. $X_{Gr} = Ca/(Ca+Fe+Mg+Mn)$. (B) Diopside. $X_{Mg} = Mg/(Mg+Fe)$. Al cations are calculated for six oxygens (see Table 2). (C) Hornblende. $X_{Mg} = Mg/(Mg+Fe)$. (Na + K), Ca and Al cations are calculated for 23 oxygen equivalents (see Table 3). (D) Plagioclase. $X_{An} = Ca/(Ca+Na+K)$.

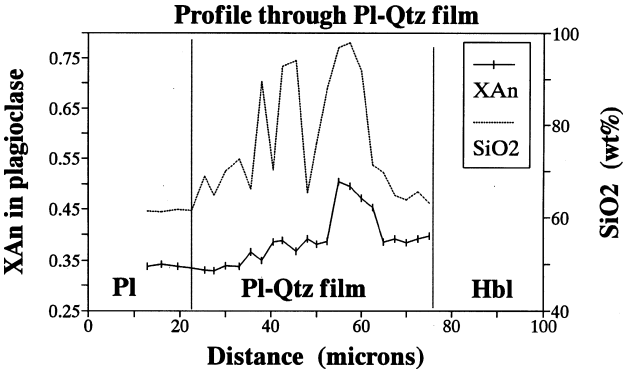

Fig. 7. Electron microprobe profile through the long dimension of a plagioclase–quartz film, similar to that illustrated in Fig. 5(F). The profile starts in plagioclase and finishes in hornblende.

(Pattison & Newton, 1989); 730 (700–750) Berman (1991, June, 1992 update); and 710 (685–725) (Aranovich & Pattison, 1994; Berman *et al.*, 1995).

Regardless of calibration, we consider that these temperatures are unlikely to represent peak conditions owing to the likelihood of Fe-Mg resetting (cf. Frost & Chacko, 1989; Pattison & Bégin, 1994) during the slow cooling of the KSZ (Percival & Peterman, 1994). The core-rim pattern of increasing Mg/(Mg + Fe) in diopside and decreasing Mg/(Mg + Fe) in garnet indicates obvious down-temperature Fe-Mg exchange in the rims. Flat Fe-Mg profiles in the interior of garnet and diopside grains that preserve irregular core-rim variations of X_{Ca} and Al cations, respectively, may also indicate resetting of Fe-Mg in the interior of the grains (see Pattison & Bégin, 1994).

Further evidence for Fe-Mg resetting comes from evaluation of the calculated temperatures with respect to experimentally constrained petrogenetic grids. A large body of experimental data on natural and synthetic starting compositions indicates that the minimum temperature for vapour-absent dehydration melting of K-poor amphibolite over a wide pressure interval (3–15 kbar) is 850–900 °C (Ellis & Thompson, 1986; Hacker, 1990; Beard & Lofgren, 1991; Rushmer, 1991; Rapp *et al.*, 1991; Wolf & Wyllie, 1991, 1993; Sen & Dunn, 1994; Thompson & Ellis, 1994; Patiño-Douce & Beard, 1995). Patiño-Douce & Beard (1995) found that a dry quartz-bearing mixture of hornblende and plagioclase, close in composition to hornblende and plagioclase in the Kapuskasing gneisses, began to undergo dehydration melting between 880 and 900 °C at 10 kbar. The occurrence of the subassemblage Grt + Opx ± Bt ± Kfs in paragneisses interlayered with mafic gneiss near the study area (Percival, 1983) suggests a minimum temperature of about 860 °C at

Table 6. Pressure-temperature estimates from Grt-Di-Pl-Qtz thermobarometry.

		Temperature (°c)				Pressure (kbar)						
		for calculated P				for calculated T			for T = 850 °C			
	$\ln(K_d)$ (Grt-Di)	EG	PN	B	BAP	B	ENK	MEA*	B*	ENK	MEA*	B $a_{SiO_2}=0.8$
SA1-3a	1.97	745	635	735	710	9.3	9.3	9.6	11.0	9.9	11.2	10.1
SA1-4a	1.96	765	660	750	725	9.6	9.3	9.9	11.2	9.8	11.4	10.3
SA1-8	1.93	745	650	735	715	9.3	9.3	9.6	11.0	9.8	11.2	10.1
SA1-12	2.00	735	630	715	700	8.9	9.0	9.5	10.9	9.5	10.9	10.0
SA1-13a	2.02	725	615	700	685	8.5	8.7	9.3	10.7	9.2	10.7	9.8
Average	1.98	745	640	730	710	9.1	9.1	9.6	11.0	9.6	11.1	10.1

B—Berman (1988, 1991; June 1992 update); BAP—Berman *et al.* (1995); EG—Ellis & Green (1979); ENK—Eckert *et al.* (1991); MEA—Moecher *et al.* (1988); PN—Pattison & Newton (1989); *average of Fe- and Mg-end-member expressions.

10 kbar (Vielzeuf & Clemens, 1992; Vielzeuf & Montel, 1994). Consequently, we consider 850 °C to be a minimum estimate of peak metamorphic temperature.

Regardless of whether 700–750 °C or 850 °C temperatures are accepted as peak conditions, any of these temperatures lies well above the water-saturated trondhjemite solidus at 10 kbar (see fig. 10 of Pattison, 1991). In the absence of regional-scale influx of low a_{H_2O} fluids, we suggest that dehydration of hornblende was accompanied by melting, consistent with the textural data.

Pressure

Taking $a_{SiO_2}=1$ and temperature estimates from garnet-diopside thermometry (685–725 °C), pressure estimates from garnet-diopside-plagioclase-quartz barometry using TWQ are very similar to those reported by Mäder *et al.* (1994), averaging 9.1 kbar (range 8.7–9.6). If the average temperature was as high as 850 °C, however, pressures increase to about 11.0 kbar (Table 6), owing to the positive slope of the equilibria used for barometry (see fig. 3 of Mäder *et al.*, 1994). This result is more consistent with experimental studies (Rapp *et al.*, 1991; Wolf & Wyllie, 1993; Patiño-Douce & Beard, 1995) that suggest minimum pressures of 10 kbar for garnet production from dehydration melting of a hornblende + plagioclase + quartz protolith.

If quartz was not present at peak conditions, a_{SiO_2} may have been lower than unity, which will affect the pressure estimate. We consider substantially reduced a_{SiO_2} at peak conditions to be unlikely, owing to the presence of abundant trondhjemitic leucosome in the rocks. If a_{SiO_2} was as low as 0.8, pressures are lowered by about 0.9 kbar relative to $a_{SiO_2}=1$, resulting in an average pressure at 850 °C of 10.1 kbar. Accepting that a_{SiO_2} was close to unity, we favour the 11.0 kbar estimate.

Activity of water

Activity of water was calculated using the method of displaced amphibole equilibria described in Mäder *et al.* (1994). The results are in the same range as the Mäder *et al.* (1994) study, in the range a_{H_2O} 0.15–0.35. If temperature was as high as 850 °C, the values increase by 0.2–0.4. Reduced activity of water is consistent with the inferred process of vapour-absent dehydration melting.

MASS BALANCE ANALYSIS

Mass balance analysis was applied to the mafic migmatites to (1) see if there are any mass balances within the rocks that provide a good model for the reaction relationships inferred from modal mineralogy and textures, and (2) search for controls on the variable extent of reaction of hornblende in the different layers.

First, the thermodynamic variance of individual samples was examined to see if there are any mass balances implied within the analytical uncertainty of the measured mineral compositions. The algebraic approach we adopted for this analysis is that of singular value decomposition (SVD) (Fisher, 1989; Gordon *et al.*, 1991). Fisher's software was used for the calculations. An example of the procedure in a simple system is described in the Appendix. The Appendix is available from: (1) the *Journal of Metamorphic Geology* World Wide Web site; (2) the British Library, via their Supplementary Publications Scheme, no. 90416; or (3) the authors. Mineral exchange vectors (Thompson, 1982a, b) were subsequently incorporated in an attempt to improve the modelling of the reactions (Hartel, 1993).

Composition of phases

Mineral phases

The mineral phases considered are hornblende, plagioclase, garnet, diopside, titanite and quartz. The compositions of the minerals are described in terms of the following 10 cations: Si, Ti, Al, Fe, Mn, Mg, Ca, Na, K and H (Tables 1–5). No distinction was made between Fe^{2+} and Fe^{3+}. F and Cl are present in negligible abundance (Tables 1–5) and have been ignored. Hornblende is assumed to contain two H

atoms, although this value is considered to be a maximum in granulites forming under conditions of reduced activity of water (see discussion below).

Melt phase

In contrast to the solid phases, whose compositions can be measured, the composition of trondhjemitic melt has to be estimated. Three different compositions were used, which are listed in Table 7. The first melt composition is based on the observed average model leucocratic mineralogy of the leucosomes now in the rocks, 40% quartz and 60% plagioclase, with an assumed plagioclase composition representative of the measured plagioclase in the leucosome, An_{35}. A reliable estimate of an aluminous ferromagnesian component in the melt was impossible to obtain owing to the lack of textural or compositional criteria to distinguish between Fe-Mg-Al minerals (garnet, diopside, hornblende) that may have been mechanically entrained in the melt segregations from those that might have crystallized from the melt. Consequently, two melt compositions were used from the experimental literature that provide analogues of the mineral and leucosome compositions at Kapuskasing: MMA Mix no. 3 from table 4 of Rushmer (1991), and Run 207 from table 3 of Beard & Lofgren (1991). Owing to uncertainty in water contents of melts produced from dehydration melting of amphibolite [Beard & Lofgren (1991) estimated water contents of 5–6 wt% whereas Rushmer (1991) estimated water contents closer to 2 wt%], we have chosen an intermediate value of 4 wt%. Following the approach of Waters (1988), melt compositions were recast into cations assuming 10 oxygens per formula unit.

Table 7. Melt compositions.

	Tdh 1	Tdh 2	B&L 91 207	Rush 91 MMA#3
SiO_2	73.36	72.60	69.54	74.21
TiO_2	0.00	0.00	0.57	1.05
Al_2O_3	14.98	14.83	14.71	13.21
FeO	0.00	0.00	2.82	2.67
MnO	0.00	0.00	0.06	0.06
MgO	0.00	0.00	0.84	0.60
CaO	4.26	4.22	3.62	1.92
Na_2O	4.40	4.35	2.93	1.46
K_2O	0.00	0.00	0.92	0.82
H_2O	3.00	4.00	4.00	4.00
Total	100.00	100.00	100.00	100.00
Si	3.820	3.752	3.655	3.828
Al	0.920	0.903	0.912	0.803
Ti	0.000	0.000	0.022	0.041
Fe	0.000	0.000	0.124	0.115
Mn	0.000	0.000	0.003	0.003
Mg	0.000	0.000	0.066	0.046
Ca	0.238	0.234	0.204	0.106
Na	0.444	0.436	0.299	0.146
K	0.000	0.000	0.062	0.054
H	1.042	1.379	1.403	1.376

Cations calculated for 10 oxygens.

Mass balance analysis using SVD

For our mass balance analysis, we chose the seven phases that account for over 99% of the mode (hornblende, plagioclase, quartz, garnet, diopside, titanite, Tdh) in the chemical system K–Na–Ca–Fe–Mg–Mn–Al–Ti–Si–H (KNCFMMnATSH) which accounts for over 99% of the oxygen-free composition of the rock. Model mass balances are listed in Table 8 for different samples and melt compositions. For each model mass balance, percentage deviations from perfect cation and charge balance are also listed (see explanation in the Appendix).

Example calculation: sample SA1-12

For sample SA1-12 and melt composition Tdh2 from Table 7, SVD analysis of the 7×10 composition matrix yields seven nonzero singular values, indicating a rank of 7 and at least divariant equilibrium (refer to Appendix). However, the smallest singular value is close to zero, opening the possibility that, within analytical uncertainties in mineral compositions, a model matrix of reduced rank (6) might provide an adequate representation of the original composition matrix. In this situation, a mass balance is implied, which for SA1-12 is:

$$1.00\ \mathrm{Hbl} + 0.72\ \mathrm{Pl} + 4.14\ \mathrm{Qtz} + 0.17\ \mathrm{Ttn} = 0.90\ \mathrm{Grt} + 1.98\ \mathrm{Di} + 1.56\ \mathrm{Tdh}. \quad (5)$$

There are a number of ways to evaluate this model mass balance. If one considers the absolute deviations from perfect cation and charge balance summed over all elements in mass balance (5), compared with that possible from analytical uncertainty alone (see example in the Appendix), the results are within three times the 1σ analytical uncertainty. Recasting this deviation as a percentage of the total number of cations and charges on one side of the model mass balance (here, the left-hand side), the deviations amount to 7.1 and 5.3%, respectively. When assessed in this way, sample SA1-12 may be viewed as preserving something close to (if not exactly) univariant equilibrium.

On the other hand, the occurrence of several elements in individual phases with residuals greater than three times the 1σ analytical uncertainty indicates that the model matrix of rank 6 is not an adequate representation of the compositional matrix, and therefore that the above mass balance is not valid (see discussion in Appendix). Deviations from perfect cation and charge balance for some major elements, such as Ca and Mg, exceed the 3σ uncertainties. Finally, a conspicuous inconsistency in mass balance (5) is the occurrence of titanite and hornblende, the only two phases with significant Ti, on the same side of the mass balance.

To address this last point, we weighted Ti by a factor of 10 in the SVD analysis, yielding the following

Table 8. Model mass balances from SVD analysis in the system KNCFMMnASTH.

Mass balance	Sample	Melt*	H atoms in Hbl/Tdh*	Model mass balances							% deviation† from perfect mass balance	
				Hbl	Pl	Qtz	Grt	Di	Ttn	Tdh	Cations	Charge
(5)	SA1-12a‡	Tdh2	2/1.379	1.00	0.72	4.14	−0.90	−1.98	0.17	−1.56	7.0	5.1
(6)	SA1-12b	Tdh2	2/1.379	1.00	0.80	4.24	−0.94	−1.76	−0.21	−1.61	7.5	4.6
(7)	SA1-8	Tdh2	2/1.379	1.00	0.79	4.17	−0.89	−1.86	−0.17	−1.61	7.8	4.7
(8)	SA1-4a	Tdh2	2/1.379	1.00	0.81	4.11	−0.94	−1.74	−0.18	−1.61	7.1	4.2
(9)	SA1-12	Rush	2/1.376	1.00	0.37	5.14	−0.73	−1.93	−0.14	−1.63	8.3	4.8
(10)	SA1-12	B&L	2/1.403	1.00	0.58	4.13	−0.79	−1.79	−0.17	−1.59	7.5	4.4
(11)	SA1-12	Tdh1	2/1.042	1.00	1.23	5.33	−0.96	−1.71	−2.17	−0.21	6.3	3.5
(12)	SA1-12	Tdh2	1/1.379	1.00	0.28	3.43	−0.88	−1.93	−0.20	−0.99	10.8	6.9

* Refer to Table 7. † See Appendix for explanation. ‡ Mass balance (5) is from an unweighted SVD analysis. All other mass balances are from SVD analysis in which Ti is weighted by a factor of 10 (see discussion in text).

mass balance:

$$1.00\ \mathrm{Hbl} + 0.80\ \mathrm{Pl} + 4.24\ \mathrm{Qtz} = 0.94\ \mathrm{Grt} + 1.76\ \mathrm{Di} + 0.21\ \mathrm{Ttn} + 1.61\ \mathrm{Tdh}. \quad (6)$$

Apart from the improvement with respect to titanite and hornblende, mass balance (6) is very similar to mass balance (5). The overall deviations from perfect cation and charge balance for mass balance (6) are 7.4 and 4.6%, respectively. The similarity of these values to those for mass balance (5) suggests that the weighting provides no worse fit to the original composition matrix than the unweighted model matrix did.

With respect to the natural rocks, mass balance (6) qualitatively accounts well for the textures and modal variations observed in the natural samples (compare with Figs 2–5 and reaction 4). Therefore, notwithstanding some of the problems noted above, mass balance (6) appears to provide a first-order model of the natural reaction.

Results for other samples and melt compositions

The above procedure was repeated for different samples and melt compositions (see Table 8). Ti was weighted by a factor of 10 in all cases. For samples SA1-8 and SA1-4a, the hornblende-richest and hornblende-poorest samples, respectively, the computed mass balances (7 and 8 in Table 8) are insignificantly different from the one for SA1-12. To examine the effect of using different melt compositions, model mass balances were calculated for SA1-12 using melt compositions MMA Mix no. 3 of Rushmer (1991) and glass 207 from Beard & Lofgren (1991), assuming 4 wt% water in the melts (mass balances 9 and 10 in Table 8). The main difference compared to mass balance (6) is the smaller coefficient of plagioclase, owing to the lower Na and Ca content of the experimental melt compositions compared with the estimated melt composition. To examine the effect of varying the H content of melt and of hornblende, model mass balances for SA1-12 were calculated with the following two changes: melt composition Tdh1 (3 wt% water) was used in place of Tdh2 (mass balance 11 in Table 8), and hornblende containing one rather than two H atoms was used with Tdh2, giving mass balance (12). Because all of the H in the melt comes from that released from the reaction of hornblende, the effect of reducing the H content of melt (mass balance 11) with no change in H content of hornblende is to increase the amount of melt produced per mole of hornblende consumed, which correspondingly results in increases in the coefficients for plagioclase and quartz. Conversely, reducing the H content of hornblende (mass balance 12) for a fixed H content in the melt results in a smaller volume of melt produced, which results in reductions in the coefficients for plagioclase and quartz.

Role of quartz

All of the above model mass balances have quartz as a reactant with a large coefficient. Considering the generally low modal abundance of quartz in metabasaltic amphibolites, and the magmatic quartz textures in the Kapuskasing rocks, availability of quartz may have been of central importance in controlling the progress of the hornblende-consuming, Grt + Di + Tdh-producing reaction.

Mass balance analysis incorporating exchange vectors

Rationale

Because the natural granulite-forming reaction in detail appears to be multivariate, an attempt was made to improve the modelling of the reaction by incorporating mineral exchange vectors (e.g. Thompson, 1982a,b; Russ-Nabelek, 1989). A complication in the modelling of multivariate reactions is that the composition of the minerals now in the rocks is not the same as the composition at the start of the reaction (neglecting the later effects of compositional modification on cooling). An indication of the variation in mineral compositions through the Grt + Di + Tdh-producing reaction may be obtained from the wide range of reaction progress in the interlayered gneisses, from hornblende-rich (small amount of reaction progress) to hornblende-

poor (large amount of reaction progress). The compositional effects related to reaction progress will be superimposed on the primary mineral compositional variability imposed by the bulk composition of the individual layers.

Evaluation of exchange components

Referring to Fig. 6, the primary chemical variations as a function of modal mineralogy include: Mg/(Mg + Fe) in garnet, diopside and hornblende; An content in plagioclase; and Al content in hornblende and to a lesser extent diopside. Numerous studies have shown that variation in Al content of hornblende mainly reflects a combination of $(Fe,Mg)_{-1}Si_{-1}Al_2$ (tschermak exchange) and $(Vac_{-1}Si_{-1}(Na,K)Al)$ ('edenite-like' exchange; Schumacher, 1991) (see studies of Raase *et al*., 1986; Russ-Nabelek, 1989; Schumacher, 1991). In the samples from Kapuskasing, the ratio of tschermak exchange to edenite-like exchange is $\approx 2:1$ (Table 3 and Fig. 6c; Hartel, 1993).

Model reactions

We chose the system Na(+K)–Ca–Fe(+Mn)–Mg–Al–Si–Ti–H (NCFMASTH) as an appropriate chemical system. Mn has been combined with Fe, and K has been combined with Na. The measured mineral compositions of sample SA1-12 and Tdh2 were selected as the additive components. Based on the above discussion, the following exchange components were included: (1) a 2:1 ratio of tschermak and edenite exchange, with Fe/Mg in the same ratio as in the hornblende ('pg'); (2) $Ca_{-1}Al_{-1}NaSi$ exchange (pl); and (3) $Fe_{-1}Mg$ exchange (fm). The 8×10 matrix of additive and exchange components is shown in Table 9. Row reduction of the matrix reveals that it has a rank of 8, with two implied independent mass balances that span reaction space (e.g. mass balances 13 and 14 in Table 9).

To obtain a single mass balance incorporating all three exchange components, mass balance (14) (which incorporates the 'pg' exchange) must be added in some proportion to mass balance (13) (which incorporates the pl and fm exchanges). Based on the maximum observed variation of Al in hornblende (*c*. 0.2 cations), addition of 0.2 times the 'pg' exchange to mass balance (13) yields the following combined mass balance:

$$1.00\ \text{Hbl} + 1.03\ \text{Pl} + 3.47\ \text{Qtz} = 1.26\ \text{Grt} + 1.44\ \text{Di} + 0.21\ \text{Ttn} + 1.43\ \text{Tdh} + 0.20\ \text{'pg'} + 0.55\ \text{fm} + 0.46\ \text{pl}. \quad (15)$$

With regard to the coefficients of the additive components, mass balance (15) shows many similarities to mass balance (6) from SVD analysis, including a large coefficient for quartz. The sense of Mg-enrichment as a function of reaction progress is consistent with constraints from natural and experimental data on amphibole stability (e.g. Wolf & Wyllie, 1993). The sense of decreasing anorthite content is consistent with the normal zoning seen in individual plagioclase grains, although quantitatively the amount of plagioclase exchange may be too high to reconcile with the observations (the amount of implied plagioclase exchange per mole of plagioclase consumed would drive the plagioclase to nearly pure albite). A second problematic aspect of mass balance (15) is the *c*. 1:1 ratio of Grt/Di produced, which seems high compared with the observed Grt/Di ratios in Fig. 3.

Optimization of mass balance analysis

Both mass balance (6) from SVD analysis and multivariate mass balance (15) are deficient in certain ways. Mass balance (6) is unsatisfactory in balancing all elements to within three sigma uncertainty (e.g. Ca and Mg). Mass balance (16), although a perfect cation and charge balance, appears to involve too much plagioclase exchange and suggests a rather high Grt/Di ratio. We have therefore combined the two approaches in an attempt to balance all elements within three sigma uncertainty using the minimum amount of multivariancy. The minimum ratio of multivariate mass balance (15) to mass balance (6) (the latter recalculated in the same eight-component system as

Table 9. Analysis of multivariant mass balances for SA1-12.

	Additive components							Exchange components		
	Hbl	Pl	Qtz	Grt	Di	Ttn	Tdh2	'pg'	fm	pl
Si	6.318	2.556	1.000	2.991	1.948	1.022	3.752	−1.000	0.000	1.000
Al	2.258	1.443	0.000	1.923	0.103	0.042	0.903	1.667	0.000	−1.000
Ti	0.216	0.000	0.000	0.002	0.006	0.964	0.000	0.000	0.000	0.000
Fe	2.325	0.003	0.000	1.912	0.372	0.020	0.000	−0.361	−1.000	0.000
Mg	1.964	0.000	0.000	0.421	0.653	0.000	0.000	−0.306	1.000	0.000
Ca	1.907	0.443	0.000	0.797	0.894	0.936	0.234	0.000	0.000	−1.000
Na	0.637	0.554	0.000	0.000	0.040	0.000	0.436	0.333	0.000	1.000
H	2.000	0.000	0.000	0.000	0.000	0.000	1.397	0.000	0.000	0.000
Two independent mass balances (normalized to 1.00 Hbl and 1.00 'pg')										
(13)	1.00	0.83	3.88	−1.27	−1.29	−0.21	−1.43		−0.59	−0.42
(14)		1.01	−2.04	0.05	−0.77	0.01		−1.00	0.17	−0.19
Massbalance (13) plus 0.2 times mass balance (14)										
(15)	1.00	1.03	3.47	−1.26	−1.44	−0.21	−1.43	−0.20	−0.55	−0.46

mass balance 15) required to balance all elements to within three sigma uncertainty is 0.71 : 0.29. The result is:

$$1.00\ \text{Hbl} + 0.92\ \text{Pl} + 3.76\ \text{Qtz} = 1.14\ \text{Grt} + 1.54\ \text{Di} + 0.21\ \text{Ttn} + 1.49\ \text{Tdh} + 0.14\ \text{`pg'} + 0.39\ \text{fm} + 0.33\ \text{pl}. \quad (16)$$

We accept mass balance (16) as the best model of the natural granulite-forming reaction.

Relation between mass balance and reaction history

Even though mass balance (16) provides a good model for the observed modal, textural and mineral chemical variations in the rocks, there is no guarantee that this reaction actually occurred in the rocks as written. Mass balance (16) may instead represent the integrated effects of a several-stage reaction history, perhaps involving a more-or-less discontinuous quartz-consuming dehydration melting reaction followed by more subtle reactions controlled by mineral exchange vectors in hornblende and plagioclase (e.g. Frost & Tracy, 1991, pp. 259–262). Our data do not allow us to distinguish between these possibilities.

Conversion to volumes

Mass balance (16) was converted to modal amounts of minerals using the following mineral volumes (values in $cm^3\ mol^{-1}$), interpolated from end-member data from Berman (1988, 1991 update): hornblende – 274.8; plagioclase – 100.8; quartz – 23.7; garnet – 117.4; diopside – 66.8; titanite – 55.7. The second-order volumetric effects of exchange components in the multivariate mass balances were ignored. Melt volumes were calculated using the procedure described by Lange (1994). For a 10-oxygen formula unit, the volume of melt composition Tdh2 containing 4 wt% water at 10 kbar, 850 °C is 129.1 cm^3 (giving a melt density of 2.4 g cm^{-3}). The modal balance is:

$$1.00\ \text{Hbl} + 0.34\ \text{Pl} + 0.32\ \text{quartz} = 0.48\ \text{Grt} + 0.37\ \text{Di} + 0.04\ \text{Ttn} + 0.70\ \text{Tdh}. \quad (17)$$

This modal balance is similar to that inferred by Beard & Lofgren (1991) in their experiments on dehydration melting of hornblende + plagioclase + quartz.

Evaluation of reaction progress in area charts

Figure 8 contains area charts showing modal changes as a function of reaction progress of reaction (17). The starting assemblage contains 35% plagioclase, two different proportions of hornblende and quartz, and 5% diopside assumed to have been inherited from lower grade (see isograd map in Percival, 1983). We assume there was no garnet in the starting composition because garnet without diopside is not reported downgrade of the garnet + diopside isograd (Percival, 1983).

The two proportions of hornblende and quartz tested are: 55% Hbl and 5% Qtz (Fig. 8a,c); and 45% Hbl and 15% Qtz (Fig. 8b,d). All area charts have vol.% leucosome produced as the measure of reaction progress. In Fig. 8(a,b), the leucosome generated is assumed to leave the rock when it is formed, and the hornblende, quartz, plagioclase, diopside, garnet and titanite are renormalized to 100%. Figure 8(c,d) illustrates the other extreme in which none of the leucosome is lost from the rock. Variation in reaction coefficients as the reaction proceeds has been ignored.

Comparison with natural modal variations

Variations in the extent of reaction of reaction (17) generally account well for the observed modal variations: garnet, diopside and titanite increase at the expense of hornblende and quartz. The plagioclase pattern in Fig. 8(a,b) is similar to that in Fig. 3, in that it shows relatively little variation as a function of modal hornblende, due to the assumption of complete extraction of trondhjemitic leucosome and consequent renormalization of the mode. In Fig. 8(c,d), in which melt is assumed to be retained in the rock, plagioclase decreases as expected. The irregular variation of quartz in Fig. 3 compared with Fig. 8 is discussed below.

Although providing a good first-order model for our observations, we do not wish to imply that all of the modal variability in the gneisses is due solely to variable reaction progress of mass balance (17) as controlled by the Hbl/Qtz ratio. Other variations in bulk composition could result in a wider range of modal proportions than implied by Fig. 8.

CONTROLS ON REACTION PROGRESS DURING DEHYDRATION MELTING

Primary control on reaction progress: abundance of quartz in the protolith

Referring to mass balance (17), modal hornblende reacts out about three times faster than quartz. Whether the system will be exhausted first in quartz or in hornblende depends on the starting composition of the Hbl + Pl + Di + Qtz protolith. Figure 8(a,c) show the situation in which quartz reacts out first, leaving a solid Hbl + Grt + Di + Pl + Ttn residue and an amount of melt (now Pl + quartz leucosome) that depends on how effectively it was removed from the reacting rock (see discussion below). Figure 8(b,d) shows the situation in which hornblende reacts out first, leaving a solid Qtz + Grt + Di + Pl + Ttn residue.

None of the rocks from the study suite is hornblende-free, suggesting that quartz in all cases reacted out first and therefore controlled the extent of reaction. Thus, a significant proportion of the modal variability between the interlayered garnet + diopside-rich and

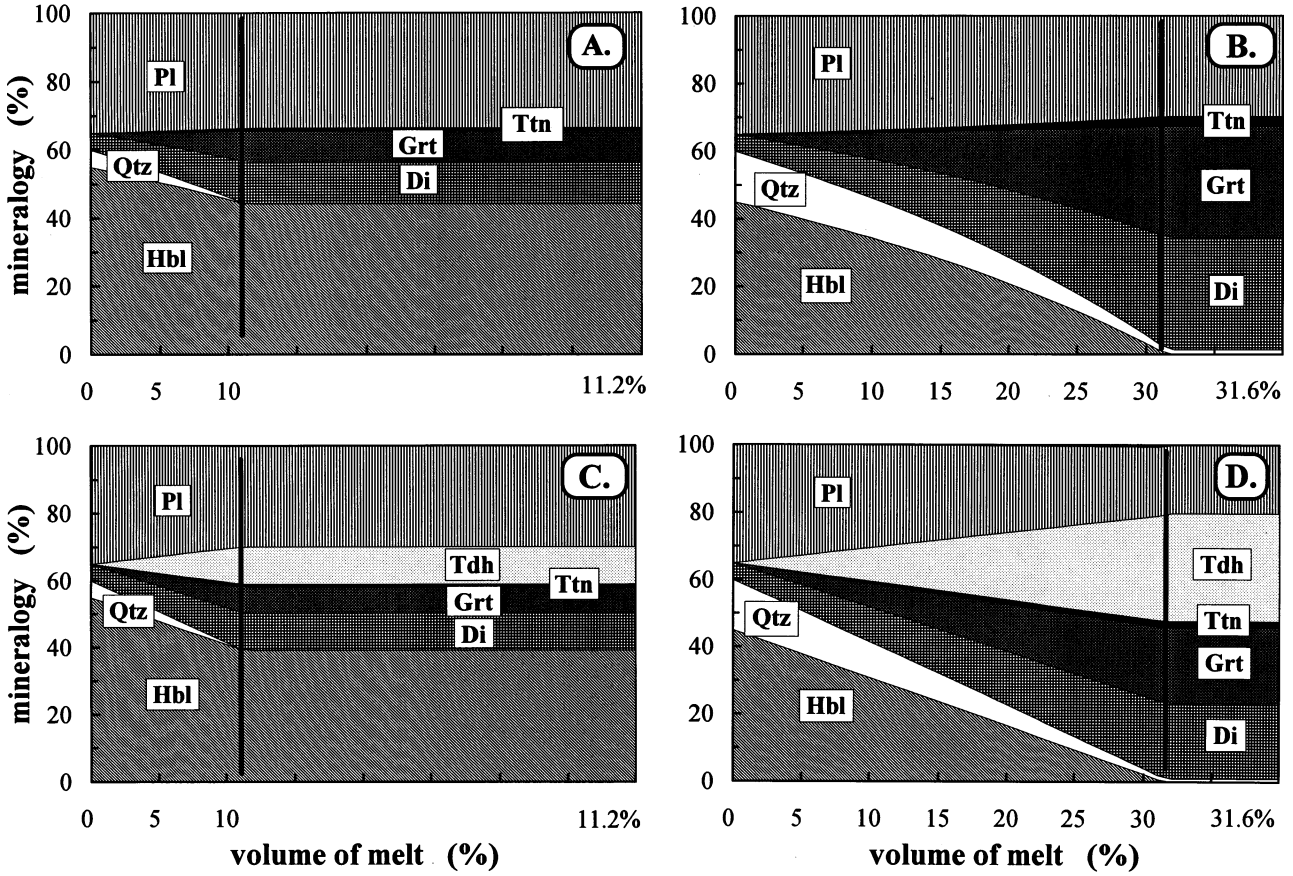

Fig. 8. Area charts showing variations in modal mineralogy as a function of reaction progress for modal mass balance (17). Reaction progress is monitored as a function of trondhjemitic leucosome produced. The solid vertical line represents the point at which a reactant (either quartz or hornblende) is consumed, causing the reaction to stall. The number at the lower right of each diagram is the vol.% leucosome produced at the point the reaction stalls. (A) Starting mineralogy – Hbl/Qtz/Pl/Di = 55 : 5 : 35 : 5. All melt is assumed to be expelled as it is produced. Quartz reacts out first, leaving a Hbl + Di + Grt + Pl + Ttn residue. (B) Starting mineralogy – Hbl/Qtz/Pl/Di = 45 : 15 : 35 : 5. All melt is assumed to be expelled as it is produced. Hornblende reacts out first, leaving a Qtz + Grt + Di + Pl + Ttn residue. (C) Same starting mineralogy as (A). All melt is assumed to be retained in the rock, resulting in the same mineral assemblage as (A) in addition to trondhjemitic leucosome. (D) Same starting mineralogy as (B). All melt is assumed to be retained in the rock, resulting in the same mineral assemblage as (B) in addition to trondhjemitic leucosome.

hornblende-rich layers may be ascribed to varying amounts of quartz in the protolith, with the quartz-richest protoliths now represented by the garnet + diopside-richest layers. Although some of the modal variability may also reflect variable modal mineralogy in the rocks prior to dehydration melting (e.g. variable abundance of diopside), the roughly proportional abundance of garnet and diopside in Fig. 3, combined with the textural data, is consistent with significant production of both minerals by the dehydration melting reaction.

Further support for the above interpretation comes from the fact that the Hbl + Grt + Di subassemblage shows a range of Fe-Mg ratios in different layers even though the rocks experienced the same P–T conditions. Neglecting the effects of other compositional variations (discussed below), if several layers contain the same mineral assemblage and equilibrated at the same P–T conditions, the Fe-Mg ratios of the minerals in all layers should in theory be the same; bulk compositional variations would be manifested in modal differences within the common assemblage. The simplest explanation is that in the KSZ rocks, the different sets of Fe-Mg ratios reflect the P–T conditions at which quartz was consumed in the reaction (Fig. 9). Although subsequent modification of the mineral compositions is indicated by the similarity in K_d(Fe-Mg) between garnet and diopside in the different layers (Table 6), indicating continued Fe-Mg exchange following stalling of the main net transfer reaction, this later exchange will have only a second-order effect on the Fe-Mg ratios of the phases over the temperature interval concerned.

Referring to Fig. 3, the amount of modal quartz in the melanosome varies from 2 to 15% and shows no consistent pattern as a function of modal hornblende. Quartz in the modes is due to the presence of interstitial quartz (e.g. Fig. 5c–e) in addition to quartz contained in subtle quartzofeldspathic segregations in the melanosome which were not recognized as such

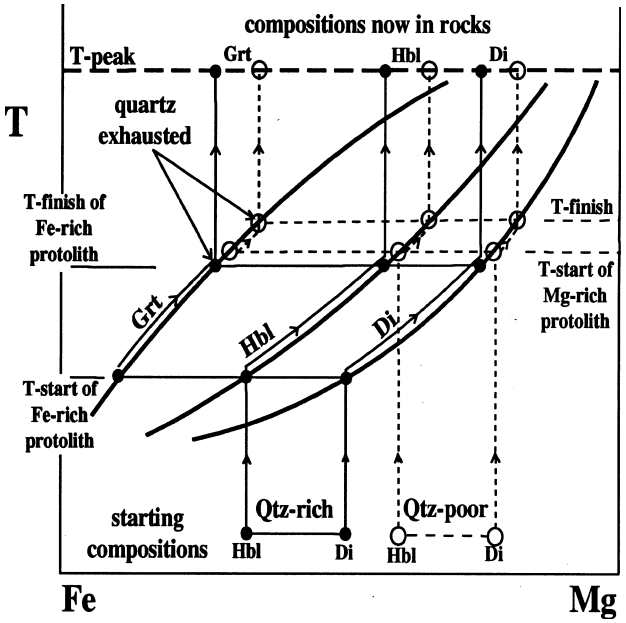

Fig. 9. Schematic T-$X_{Fe\text{-}Mg}$ diagram accounting for the observed modal mineralogy and compositional variations between mafic gneiss layers. The heavy curved lines represent schematically the sense of Mg enrichment in coexisting hornblende, garnet and diopside as a function of reaction progress through the Fe-Mg divariant reaction Hbl + Pl + Qtz = Grt + Di + Ttn + Tdh. The evolution of two representative starting Hbl + Di + Pl + Qtz assemblages are shown. Assemblage 1 (solid circles and tie-lines) is Fe-rich and quartz-rich; assemblage 2 (dashed circles and tie-lines) is Mg-rich and quartz-poor (see text for justification). Fe-rich assemblage 1 begins reaction at relatively low temperature, and undergoes substantial reaction progress, producing a Grt + Di-rich assemblage. Consumption of quartz causes the reaction to stall. Even though temperature continue to rise, the Fe-Mg ratios of hornblende, garnet and diopside record the temperature conditions at which quartz was consumed (neglecting minor up-temperature Fe-Mg exchange between hornblende, garnet and diopside following stalling of the main reaction). Mg-rich assemblage 2 begins reaction at relatively high temperature, and undergoes only a small amount of reaction progress before quartz is consumed, resulting in a hornblende-rich assemblage. As with assemblage 1, the compositions of hornblende, garnet and diopside record the temperature at which quartz was consumed. Note that if consumption of quartz did not control the extent of reaction, both of the Hbl + Grt + Di + Ttn + Pl (+ Qtz) assemblages would be constrained to the T-$X_{Fe\text{-}Mg}$ loops and would therefore record the same Fe-Mg ratios (corresponding to peak conditions).

when the point counting was done. Omission of melt-related quartz would result in the absence of quartz from the modes in Fig. 3.

Our conclusion that abundance of quartz was the primary control on reaction progress in the KSZ mafic granulites agrees with the inferences of a number of earlier field-based and experimental studies. Sen & Ray (1971) noted that a_{SiO_2} was probably of central importance in controlling the distribution of hornblende-rich and pyroxene-rich assemblages in mafic granulites from Madras. Rushmer (1991) and Sen & Dunn (1994) suggested that the type and extent of reaction in dehydration melting experiments on amphibolite was controlled by presence or absence of quartz.

Secondary controls on reaction progress: mineral compositional variations

Mineral compositional variations will have influenced the temperature of inception and progress of reaction. The most important compositional variations are Fe-Mg ratio, Al content of hornblende and X_{An} of plagioclase.

The rocks showing the greatest extent of reaction (Di + Grt-rich layers) are the Fe-richest. These layers show the poorest development of internal leucocratic segregations, suggesting that the melt that accompanied the production of abundant garnet and diopside was mechanically expelled from the rock. In contrast, the hornblende-richest layers, which are the Mg-richest, show the best development of internal leucosomes, suggesting that they may have been quenched shortly after reaction. Thus, a time sequence is implied, with the Fe-richest layers having reacted earlier than the Mg-richer layers.

An estimate of the temperature effect on the reaction for the observed range of Fe-Mg compositions can be made by calculating displacements of the following equilibrium:

$$\underset{\text{in Pl}}{3\ \text{An}} + \underset{\text{in Amp}}{4\ \text{Tr}} = \underset{\text{in Grt}}{3\ \text{Py}} + \underset{\text{in Di}}{11\ \text{Di}} + \underset{\text{Qtz}}{7\ \beta\text{-Qtz}} + 4\ H_2O \qquad (18)$$

Some imprecision is introduced owing to the fact that equilibrium (18) is a water-producing rather than melt-producing equilibrium. The TWQ software of Berman (1991; June 1992 update) and the thermodynamic data of Mäder *et al.* (1994) were used for the calculations. The position of the above equilibrium for the Fe-richest sample, SA1-4a, occurs 40 °C lower than for one of the Mg-richest samples, SA1-12, consistent with the textural observations. Continued Fe-Mg exchange following stalling of the net transfer reaction introduces a small component of uncertainty in the estimate. A second complication is that the mineral compositions now present in the rocks will have evolved to more Mg-rich compositions during progress of the net transfer reaction (e.g. Wolf & Wyllie, 1993). If so, the mineral compositions at the onset of reaction may have been Fe-richer, with the effect increasing as a function of reaction progress. Surprisingly, the layers showing the greatest extent of reaction contain the Fe-richest mineral compositions, even though the minerals in these layers will have experienced the greatest amount of Mg-enrichment as a function of reaction progress. This suggests that the quartz (SiO_2)-richest layers also had the highest Fe/(Fe + Mg) ratios, in agreement with the whole-rock chemical data of Percival (1986).

The effects of the observed range of plagioclase composition and Al content of hornblende were similarly estimated using equilibrium (22). Varying the X_{An} content of plagioclase by $\pm 5X_{An}$ results in a displacement of $\pm 15\,^{\circ}C$, whereas varying the Al content of amphibole by ± 0.1 cations (accompanied by variation in Si, Mg, Fe, Na, and K appropriate to the 'pg' exchange) results in a displacement of $\pm 20\,^{\circ}C$.

Combining all of the compositional effects for the observed range of mineral compositions, the onset of the reaction could have varied by as much as about $75\,^{\circ}C$, with the lowest temperatures being for Fe-rich layers containing Al-poor hornblende and An-rich plagioclase. This spread of temperatures is greater than implied by Beard & Lofgren (1991), who found that the inception of dehydration melting was apparently insensitive to the composition of the starting amphibole and plagioclase.

It is important to note that mineral compositional variation alone cannot account for the differing extents of reaction observed in the gneisses. Fe-rich hornblende still remains in the Grt + Di-rich layers (e.g. SA1-4b), even though it should have reacted out had there been any solid quartz available. The hornblende is not enriched in minor components (e.g. F) that might have stabilized it (Table 3). Plagioclase in these layers, although strongly zoned, is relatively calcic which would favour rather than retard reaction.

EXPULSION OF MELT

Figure 8 shows opposite extremes in the assumed extent to which trondhjemitic leucosome was expelled from the rocks. In these models, 10–35% leucosome is generated, depending on the amount of quartz in the protolith. In outcrop, apart from rocks containing obviously intrusive veins and dykes, most layers contain 5–10 vol.% leucosome, sometimes as high as 20% in the hornblende-richer layers (Fig. 2). These variations imply variable extents of expulsion of the melt intermediate between the two extremes. The small amount of leucosome in the Grt + Di-richest layers suggests that melt generation and expulsion in these layers may have occurred prior to leucosome generation in the hornblende-rich layers. Evidence for melt expulsion and transport comes from the abundant transecting trondhjemitic veins and dykes within the gneisses.

Numerous studies have used rare earth element (REE) and trace element data from Archaean trondhjemitic and tonalitic intrusive bodies to make inferences on the source rocks for the magmas (e.g. Rudnick & Taylor, 1986; Sylvester *et al*., 1986; Rapp *et al*., 1991; Luais & Hawkesworth, 1994; and references therein). Rudnick & Taylor (1986), Rapp *et al*. (1991) and Luais & Hawkesworth (1994) concluded that a Grt ± Di ± Amp-bearing mafic granulite or eclogite is the most likely source rock to produce the highly fractionated, heavy REE-depleted signatures of many trondhjemites and tonalities. Modelling by Rudnick & Taylor (1986) and Rapp *et al*. (1991) suggested that about 20% melting from such mafic rocks could account for the observed REE patterns. Based on our mass balance modelling, we estimate that 5–35 vol.% trondhjemitic leucosome was generated during production of the Grt + Di-bearing KSZ mafic gneisses, of which most (5–30%) was expelled. These figures agree well with the inferences from REE modelling. The inferred amount of melting (4–25%) and modal mineralogy of the residue (15–45% plagioclase, 30–50% hornblende, 2–35% diopside, 3–15% garnet) inferred in the study of Luais & Hawkesworth (1994) is remarkably similar to the observed modes in our study.

ACKNOWLEDGEMENTS

This article represents part of an MSc thesis prepared by T.H.D.H. at the University of Calgary under the supervision of D.R.M.P. We express our thanks to J.A. Percival, who introduced us to the KSZ during several field excursions, and who reviewed the first draft of the paper. E.W. Sawyer, J.S. Beard and especially B.R. Frost are thanked for their formal reviews. J. Machacek, D. Glatiotis, J. Resultay, M. Horvath and B. Fong provided us with excellent technical assistance. This research was supported by NSERC research grant 037233 to D.R.M.P. and by a grant from the Geological Survey of Ontario.

REFERENCES

Aranovich, L. Ya. & Pattison, D. R. M., 1994. Reassessment of the garnet-clinopyroxene Fe-Mg exchange thermometer: I. Reanalysis of the Pattison and Newton (1989) run products. *Contributions to Mineralogy and Petrology*, **119,** 16–29.

Ashworth, J. R., 1976. Petrogenesis of migmatites in the Huntly Portsoy area, north-east Scotland. *Mineralogical Magazine*, **40,** 661–682.

Ashworth, J. R., 1985. Introduction. In: *Migmatites* (ed. Ashworth, J. R.), pp. 1–35. Blackie, Glasgow.

Beard, J. S., 1990. Partial melting of metabasites in the contact aureoles of gabbroic plutons in the Smartville Complex, Sierra Nevada, California. In: *The Nature and Origin of Cordilleran Magmatism* (ed. Anderson, J.L.), *Geological Society of America Memoir*, **174,** 303–313.

Beard, J. S. & Lofgren, G. E., 1991. Dehydration melting and water-saturated melting of basaltic and andesitic greenstones and amphibolites at 1, 3, and 6.9 kbar. *Journal of Petrology*, **32,** 365–401.

Bégin, N. J. & Pattison, D. R. M., 1994. Metamorphic evolution of granulites in the Minto Block, northern Quebec: extraction of peak *P–T* conditions taking account of late Fe-Mg exchange. *Journal of Metamorphic Geology*, **12,** 411–428.

Berman, R. G., 1988. Internally consistent thermodynamic data for minerals in the system Na_2O-K_2O-CaO-MgO-FeO-Fe_2O_3-Al_2O_3-SiO_2-TiO_2-H_2O-CO_2. *Journal of Petrology*, **29,** 445–522.

Berman, R. G., 1991. Thermobarometry using multi-equilibrium calculations: a new technique, with petrological applications. *Canadian Mineralogist*, **29,** 833–855.

Berman, R. G., Aranovich, L. Ya. & Pattison, D. R. M., 1995. Reassessment of the garnet-clinopyroxene Fe-Mg exchange thermometer: II. Thermodynamic analysis. *Contributions to Mineralogy and Petrology*, **119,** 30–42.

Brown, G. C. & Fyfe, W. S., 1970. The production of granitic melts during ultrametamorphism. *Contributions to Mineralogy and Petrology*, **28,** 310–318.

Brown, M., 1979. The petrogenesis of the St. Malo migmatite belt, Armorican Massif, France, with particular reference to the diatexites. *Neues Jahrbuch für Mineralogie Abh.*, **135,** 48–74.

Bursnall, G. T., Leclair, A. D., Moser, D. E. & Percival, J. A., 1994. Structural correlation within the Kapuskasing uplift. *Canadian Journal of Earth Sciences*, **31,** 1081–1095.

Clemens, J. D. & Vielzeuf, D., 1987. Constraints on melting and magma production in the crust. *Earth and Planetary Science Letters*, **86,** 287–306.

Corfu, F., 1987. Inverse age stratification in the Archean crust of the Superior province: evidence for infra- and subcrustal accretion from high resolution U-Pb zircon and monazite ages. *Precambrian Research*, **36,** 259–275.

Cosca, M. A., Essene, E. J. & Bowman, J. R., 1991. Complete chemical analyses of metamorphic hornblendes: implications for normalizations, calculated H_2O activities and thermobarometry. *Contributions to Mineralogy and Petrology*, **108,** 472–484.

Eckert, J. O., Newton, R. C. & Kleppa, O. J., 1991. The DH of reaction and recalibration of garnet-pyroxene-plagioclase-quartz geobarometers in the CMAS system by solution calorimetry. *American Mineralogist*, **76,** 148–160.

Ellis, D. J. & Green, D. H., 1979. An experimental study of the effect of Ca upon garnet-clinopyroxene Fe-Mg exchange equilibria. *Contributions to Mineralogy and Petrology*, **71,** 13–22.

Ellis, D. J. & Thompson, A. B., 1986. Subsolidus and partial melting reactions in the quartz-excess $CaO + MgO + Al_2O_3 + SiO_2 + H_2O$ system under water-excess and water-deficient conditions to 10 kb: some implications for the origin of peraluminous melts from mafic rocks. *Journal of Petrology*, **27,** 91–121.

Fisher, G. W., 1989. Matrix analysis of metamorphic mineral assemblages and reactions. *Contributions to Mineralogy and Petrology*, **102,** 69–77.

Frost, B. R. & Chacko, T., 1989. The granulite uncertainty principle: Limitations on thermobarometry in granulites. *Journal of Geology*, **97,** 435–450.

Frost, B. R. & Tracy, R. J., 1991. Phase equilibria and thermobarometry of calcareous, ultramafic and mafic rocks, and iron formations. In: *Contact Metamorphism* (ed. Kerrick, D. M.), *Mineralogical Society of America Reviews in Mineralogy*, **26,** 207–320.

Geis, W. T., Cook, F. A., Green, A. G., Percival, J. A., West, G. F. & Milkereit, B., 1990. Thin thrust sheet formation of the Kapuskasing structural zone revealed by LITHOPROBE seismic reflection data. *Geology*, **18,** 513–516.

Gordon, T. M., Ghent, E. D. & Stout, M. Z., 1991. Algebraic analysis of the biotite-sillimanite isograd in the File Lake area, Manitoba. *Canadian Mineralogist*, **29,** 673–686.

Grant, J. A. & Frost, B. R., 1990. Contact metamorphism and partial melting of pelitic rocks in the aureole of the Laramie anorthosite complex, Morton Pass, Wyoming. *American Journal of Science*, **290,** 425–427.

Hacker, B. R., 1990. Amphibolite facies-to-granulite facies reactions in experimentally deformed, unpowdered amphibolite. *American Mineralogist*, **75,** 1349–1361.

Hanes, J. A., Archibald, D. A., Queen, M. & Farrar, E., 1994. Constraints from $^{40}Ar/^{39}Ar$ geochronology on the tectonothermal history of the Kapuskasing uplift in the Canadian Superior province. *Canadian Journal of Earth Sciences*, **31,** 1146–1171.

Harte, B., Pattison, D. R. M. & Linklater, C. M., 1991. Field relations and petrography of partially melted pelitic and semipelitic rocks. In: *Equilibrium and Kinetics in Contact Metamorphism: the Ballachulish Igneous Complex and its Thermal Aureole* (eds Voll, G., Töpel, J., Pattison, D. R. M. & Seifert, F.), pp. 181–210. Springer Verlag, Heidelberg.

Hartel, T. H. D., 1993. Genesis of mafic migmatites from the Kapuskasing Structural Zone, Ontario, Canada. *MSc Thesis, University of Calgary, Canada.*

Johannes, W., 1983. Metastable melting in granite and related systems. In: *Migmatites, Melting and Metamorphism* (eds Atherton, M. P. & Gribble, C. D.), pp. 27–36. Shiva, Nantwich, England.

Jurewicz, S. R. & Watson, E. B., 1984. Distribution of partial melt in a felsic system: the importance of surface energy. *Contributions to Mineralogy and Petrology*, **85,** 25–29.

Kretz, R., 1983. Symbols for rock-forming minerals. *American Mineralogist*, **68,** 277–279.

Krogh, T. E. & Moser, D. E., 1994. U-Pb zircon and monazite ages from the Kapuskasing uplift: age constraints on deformation within the Ivanhoe Lake fault zone. *Canadian Journal of Earth Sciences*, **31,** 1096–1103.

Lange, R. A., 1994. The effect of H_2O, CO_2 and F on the density and viscosity of silicate melts. In: *Volatiles in Magmas* (eds Carroll, M. R. & Holloway, J. R.), *Mineralogical Society of America, Reviews in Mineralogy*, **30,** 331–370.

Luais, B. & Hawkesworth, C. J., 1994. The generation of continental crust: an integrated study of crust-forming processes in the Archean of Zimbabwe. *Journal of Petrology*, **35,** 43–93.

Mäder, U. K., Percival, J. A. & Berman, R. G., 1994. Thermobarometry of garnet-clinopyroxene-hornblende granulites from the Kapuskasing structural zone. *Canadian Journal of Earth Sciences*, **31,** 1134–45.

Mehnert, K. R., Busch, W. & Schneider, G., 1973. Initial melting at grain boundaries of quartz and feldspar in gneisses and granulites. *Neues Jahrbuch für Mineralogie Monatshefte*, **1973,** 165–183.

Moecher, D. P., Essene, E. J. & Anovitz, L. M., 1988. Calculation and application of clinopyroxene-garnet-plagioclase-quartz geobarometers. *Contributions to Mineralogy and Petrology*, **100,** 92–106.

Nicholls, J. & Stout, M. Z., 1988. Picritic melts in Kiluaea – evidence from the 1967–1968 Halemaumau and Hiiaka eruptions. *Journal of Petrology*, **29,** 1031–1057.

Nyman, M. W., Pattison, D. R. M. & Ghent, E. D., 1995. Melt extraction during formation of K-feldspar + sillimanite migmatites, west of Revelstoke, British Columbia. *Journal of Petrology*, **36,** 351–372.

Paquet, J. & Francois, P., 1980. Experimental deformation of partially melted granitic rocks at 600–900 °C and 250 MPa confining pressure. *Tectonophysics*, **68,** 131–146.

Patiño-Douce, A. E. & Beard, J. S., 1995. Dehydration-melting of biotite gneiss and quartz amphibolite from 3 to 15 kbar. *Journal of Petrology*, **36,** 707–738.

Patiño-Douce, A. E. & Johnson, A. D., 1991. Phase equilibria and melt productivity in the pelitic system: implications for the origin of peraluminous granitoids and aluminous granulites. *Contributions to Mineralogy and Petrology*, **107,** 202–218.

Pattison, D. R. M., 1991. Infiltration-driven dehydration and anatexis in granulite facies metagabbro, Grenville Province, Ontario, Canada. *Journal of Metamorphic Geology*, **9,** 315–332.

Pattison, D. R. M. & Bégin, N. J., 1994. Compositional maps of metamorphic orthopyroxene and garnet: evidence for a hierarchy of closure temperatures and implications for geothermometry of granulites. *Journal of Metamorphic Geology*, **12,** 387–410.

Pattison, D. R. M. & Harte, B., 1988. Evolution of structurally contrasting anatectic migmatites in the 3-kbar Ballachulish aureole, Scotland. *Journal of Metamorphic Geology*, **6,** 475–494.

Pattison, D. R. M. & Newton, R. C., 1989. Reversed experimental calibration of the garnet-clinopyroxene Fe-Mg exchange thermometer. *Contributions to Mineralogy and Petrology*, **101,** 87–103.

Percival, J. A., 1983. High-grade metamorphism in the Chapleau-Foleyet area, Ontario. *American Mineralogist*, **68,** 667–686.

Percival, J. A., 1986. The Kapuskasing uplift: Archean greenstones and granulites. *Geological Association of Canada, Ottawa 1986 meeting, Field trip 16 guidebook.*

Percival, J. A. & Card, K. D., 1983. Archean crust as revealed in the Kapuskasing uplift, Superior province, Canada. *Geology*, **11,** 323–326.

Percival, J. A. & Peterman, Z. E., 1994. Rb-Sr biotite and whole rock data from the Kapuskasing uplift and their bearing on the cooling and exhumation history. *Canadian Journal of Earth Sciences*, **31,** 1172–1181.

Percival, J. A. & West, G. F., 1994. The Kapuskasing uplift: a geological and geophysical synthesis. *Canadian Journal of Earth Sciences,* **31,** 1256–1286.

Powell, R., 1983. Fluids and melting under upper amphibolite facies conditions. *Journal of Geological Society of London*, **140,** 629–633.

Raase, P., Raith, M., Ackermand, D. & Lal, R. K., 1986. Progressive metamorphism of mafic rocks from greenschist to granulite facies in the Dharwar craton of southern India. *Journal of Geology*, **94,** 261–282.

Rapp, R. P., Watson, E. B. & Miller, C. F., 1991. Partial melting of amphibolite/eclogite and the origin of Archean trondhjemites and tonalites. *Precambrian Research*, **51,** 1–25.

Robinson, P., Spear, F. S., Schumacher, J. C., Laird, J., Klein, C., Evans, B. W. & Doolan, B. L., 1982. Phase relations of metamorphic amphiboles: natural occurrence and theory. In: *Amphiboles: Petrology and Experimental Phase Relations* (eds Veblen, D. R. & Ribbe, P. H.), *Mineralogical Society of America, Reviews in Mineralogy*, **9B,** 1–227.

Rudnick, R. L. & Taylor, S. R., 1986. Geochemical constraints on the origin of Archean tonalitic-trondhjemitic rocks and implications for lower crustal composition. In: *The Nature of the Lower Continental Crust* (eds Dawson, J. B., Carswell, D. A., Hall, J. & Wedepohl, K. H.), *Geological Society of London, Special Publication*, **24,** 179–191.

Rushmer, T., 1991. Partial melting of two amphibolites: contrasting experimental results under fluid-absent conditions. *Contributions to Mineralogy and Petrology*, **107,** 41–59.

Russ-Nabelek, C., 1989. Isochemical contact metamorphism of mafic schist, Laramie anorthosite complex, Wyoming: amphibole compositions and reactions. *American Mineralogist*, **74,** 530–548.

Sawyer, E. W., 1991. Disequilibrium melting and the rate of melt-residuum separation during migmatisation of mafic rocks from the Grenville Front, Quebec. *Journal of Petrology*, **32,** 701–738.

Schumacher, R., 1991. Composition and phase relations of calcic amphiboles in epidote- and clinopyroxene-bearing rocks of the amphibolite and lower granulite facies, central Massachusetts, U.S.A. *Contributions to Mineralogy and Petrology*, **108,** 196–211.

Sen, C. & Dunn, T., 1994. Dehydration melting of a basaltic composition amphibolite at 1.5 and 2.0 GPa: implications for the origin of adakites. *Contributions to Mineralogy and Petrology*, **117,** 394–409.

Sen, S. K. & Ray, S., 1971. Hornblende-pyroxene granulites vs. pyroxene granulites: a study from the type charnockite area. *Neues Jahrbuch fur Mineralogie Abh.*, **115,** 291–314.

Sylvester, P. J., Attoh, K. & Schultz, K. J., 1986. Did anatexis in the Kapuskasing structural zone produce the HREE depleted dacites of the Michipicoten greenstone belt? *Geological Association of Canada – Mineralogical Association of Canada Annual meeting, Abstracts with program*, **11,** 133.

Tait, R. E. & Harley, S. L., 1988. Local processes involved in the generation of migmatites within mafic granulites. *Transactions of the Royal Society of Edinburgh: Earth Sciences*, **79,** 209–222.

Thompson, A. B., 1982. Dehydration melting of pelitic rocks and the generation of H_2O-undersaturated granitic liquids. *American Journal of Science*, **282,** 1567–1595.

Thompson, A. B. & Ellis, D. J., 1994. $CaO + MgO + Al_2O_3 + SiO_2 + H_2O$ to 35 kbar: amphibole, talc, and zoisite dehydration and melting reactions in the silica-excess part of the system and their possible significance in subduction zones, amphibolite melting, and magma fractionation. *American Journal of Science*, **294,** 1229–1289.

Thompson, J. B., 1982a. Composition space: an algebraic and geometric approach. In: *Characterization of Metamorphism Through Mineral Equilibria* (ed. Ferry, J. M.), *Mineralogical Society of America, Reviews in Mineralogy*, **10,** 1–32.

Thompson, J. B., 1982b. Reaction space: an algebraic and geometric approach. In: *Characterization of Metamorphism Through Mineral Equilibria* (ed. Ferry, J. M.), *Mineralogical Society of America, Reviews in Mineralogy*, **10,** 33–52.

Thurston, P. C., Siragusa, G. M. & Sage, R. P., 1977. Geology of the Chapleau area. *Ontario Division of Mines, Geoscience Report*, **157**.

Vernon, R. H. & Collins, W. J., 1988. Igneous microstructures in migmatites. *Geology*, **16,** 1126–1129.

Vielzeuf, D. & Clemens, J. D., 1992. The fluid-absent melting of phlogopite + quartz: experiments and models. *American Mineralogist*, **77,** 1206–1222.

Vielzeuf, D. & Montel, J. M., 1994. Partial melting of metagreywackes. Part, I. Fluid-absent experiments and phase relationships. *Contributions to Mineralogy and Petrology*, **117,** 375–393.

Waters, D. J., 1988. Partial melting and the formation of granite facies assemblages in Namaqualand, South Africa. *Journal of Metamorphic Geology*, **6,** 387–404.

Williams, M. L., Hanmer, S. K., Darrach, M. & Kopf, C., 1995. Syntectonic generation and segregation of tonalitic melts from amphibolite dikes in the lower crust, Chipman dike swarm, northern Saskatchewan. *Journal of Geophysical Research*, **100–B8,** 15,717–15,734.

Wolf, M. B. & Wyllie, P. J., 1991. Dehydration-melting of solid amphibolite at 10 kbar: textural development, liquid interconnectivity and applications to the segregation of magmas. *Mineralogy and Petrology*, **44,** 151–179.

Wolf, M. B. & Wyllie, P. J., 1993. Garnet growth during amphibolite anatexis: implications of a garnetiferous restite. *Journal of Geology*, **101,** 357–373.

Received 31 October 1995; revision accepted 8 April 1996.